# Intermediate mass Higgs boson at the proposed CERN LEP⊗LHC *ep* collider II. Minimal supersymmetric standard model

Ghadir Abu Leil
*Department of Physics, University of Durham, South Road, Durham DH1 3LE, United Kingdom*

Stefano Moretti*
*Department of Physics, University of Durham, South Road, Durham DH1 3LE, United Kingdom and Dipartimento di Fisica Teorica, Università di Torino, and INFN, Sezione di Torino, V. Pietro Giuria 1, 10125 Torino, Italy*

(Received 24 July 1995)

The production of the MSSM Higgs bosons $H^0$, $h^0$, $A^0$, and $H^\pm$, in the intermediate mass range of the $A^0$, at two different values of $\tan\beta$, is studied at the possible CERN LEP⊗LHC *ep* collider, through $\gamma p$ interactions, by photons generated via Compton back scattering of laser light. Signatures in which $H^0$, $h^0$, $A^0 \to b\bar{b}$ and $H^\pm \to \tau\nu_\tau$ are considered. Flavor identification on $b$ jets is assumed. Backgrounds to Higgs signals are computed. Explicit formulas for the helicity amplitudes of the Higgs processes are given.

PACS number(s): 14.80.Bn, 13.60.Fz, 14.65.Fy, 14.80.Ly

## INTRODUCTION

We know that, despite its innumerable experimental successes, the standard model (SM) [1] cannot be a fundamental theory valid up to an arbitrary[1] energy scale $\Lambda$. It should rather be regarded as an effective low energy model, which has to be replaced at an energy close to the Fermi scale $G_F^{-1/2} \approx 300$ GeV by some more fundamental theory. This can be seen from the fact that, for $\Lambda \gg G_F^{-1/2}$, the one-loop radiative corrections to the SM Higgs boson mass $M_\phi$ are quadratically divergent (naturalness or hierarchy problem) [2].

Supersymmetric (SUSY) models can solve this. The most intriguing among them is probably the minimal supersymmetric standard model (MSSM) [3]. It incorporates two complex Higgs boson doublets of fundamental scalar fields $(H_1^0, H_1^-)$ and $(H_2^+, H_2^0)$, which, after a spontaneous symmetry breaking, originate five Higgs bosons: the $CP$-even neutral $H^0$ and $h^0$, the $CP$-odd neutral $A^0$, and the charged[2] $H^\pm$'s. The attractions of the MSSM are numerous. It is a predictive model: all masses and couplings in the Higgs sector can be expressed at the tree level in terms of only two real parameters, the ratio of the vacuum expectation values $v_1$ and $v_2$ of the two doublets (i.e., $\tan\beta = v_2/v_1$) and the mass of one of the bosons (e.g., $M_{A^0}$), and, at the same time, the radiative corrections can be kept well under control. It breaks the gauge symmetry close to the electroweak scale $G_F^{-1/2}$ and, if combined with grand unification theories (GUT's), it predicts a value for the Weinberg angle $\theta_W$ in good agreement with the measured one and a value for the grand unification mass $M_{\rm GUT}$ which can explain the not-observed proton decay [4]. It supplies a natural candidate for the dark matter in terms of the lightest supersymmetric particle (LSP), which is stable, neutral and weakly interacting (i.e., neutralino). Finally, so far, it survived stringent experimental constrains: e.g., the most part of its parameter space has not yet been excluded by LEP data [5].

While upper limits on the MSSM Higgs boson masses can be deduced by arguments connected with the request of unitarity of the theory, which implies that at least one neutral MSSM Higgs boson most have mass below $\sim 1$ TeV [6–8], lower limits can be extracted at present colliders. From LEP I ($\sqrt{s}_{ee} = M_{Z^0}$) experiments, as a result of searches for $e^+e^- \to Z^{0*}h^0$ and $e^+e^- \to h^0A^0$ events, one obtains [5]

$$M_{h^0} \gtrsim 44.5 \text{ GeV} \text{ and } M_{A^0} \gtrsim 45 \text{ GeV}. \quad (1)$$

Extensive studies have been carried out on the detectability of MSSM Higgs boson particles by the next generation of high energy machines, both at a $pp$ hadron collider [6,9,10] and at an $e^+e^-$ Next Linear Collider (NLC) [6,11–15].

The region $M_{A^0} < 80$–$90$ GeV will be studied at the CERN $e^+e^-$ collider LEP II ($\sqrt{s}_{ee} = 170$–$190$ GeV), by the Higgs boson decay channel $b\bar{b}$ [11], via one or both the processes $e^+e^- \to Z^{0*} \to Z^0h^0$ (bremsstrahlung) and $e^+e^- \to Z^{0*} \to h^0A^0$ (neutral pair production) [16].

Higgs bosons with larger masses will be searched

*Present address: Cavendish Laboratory, University of Cambridge, Madingley Road, Cambridge, CB3 0HE, U.K.

[1] A scale which has to be less than the Planck scale $M_{\rm Planck} \sim 10^{19}$, where a description which includes quantum gravity is needed.

[2] The three neutral Higgs states of the MSSM will be collectively indicated by the symbol $\Phi^0$.

 ©1996 The American Physical Society

for at $pp$ colliders such as the CERN Large Hadron Collider[3] (LHC), with $\sqrt{s}_{pp} = 10$, 14 TeV and $\mathcal{L} \approx 10$–100 fb$^{-1}$, or at $e^+e^-$ NLC's, with $\sqrt{s}_{ee} = 300$–2000 GeV and $\mathcal{L} \approx 10$–20 fb$^{-1}$.

At the LHC, because of the huge QCD background, the mass range 80 GeV$\lesssim M_{\Phi_0} \lesssim$ 130 GeV is the most difficult to study since in this case a neutral Higgs boson mainly decays to $b\bar{b}$ pairs, for a large choice of the MSSM parameters. However, studies have shown that the discovery of a neutral Higgs boson via the $\Phi^0 \to \gamma\gamma$ mode at hadron colliders can be exploited for the discovery of $H^0$ for 80 GeV$\lesssim M_{A^0} \lesssim$ 100 GeV and of $h^0$ for $M_{A^0} \gtrsim 170$ GeV, at all tan$\beta$. For heavier masses, the "gold-plated" decay channel ($\Phi^0 \to 4l$) is useful for the $H^0$ if tan$\beta \lesssim 7$ and 100 GeV$\lesssim M_{A^0} \lesssim$ 300 GeV, but not for the $h^0$ because of its too light mass.[4] Recently, it has been also shown [17] that with the $b$-tagging capabilities [18] of the LHC experiments,[5] it might be possible to rely, over a substantial portion of the parameter space, on the $t\bar{t}\Phi^0$ production channel, with one $t$ decaying semileptonically and $\Phi^0 \to b\bar{b}$, for 80 GeV$\lesssim M_{\Phi^0} \lesssim$ 130 GeV, for at least one of the MSSM Higgs bosons $h^0$ or $H^0$, removing the "window of unobservability" for 100 GeV$\lesssim M_{A^0} \lesssim 170$ GeV and tan$\beta \gtrsim 2$, which remained in previous analyses. Moreover, it has been found [19] also that the reaction $bg \to bZ^0\Phi^0$ is an excellent candidate for the discovery of $A^0$ and at least one of the other two neutral Higgs bosons over the whole intermediate range of $M_{A^0}$ for large values of tan$\beta$, through the same decay channel $\Phi^0 \to b\bar{b}$. With respect to charged Higgs bosons, for low (high) values of $M_{H^\pm}$ the dominant production mechanism is $gg \to t\bar{t} \to H^+H^-b\bar{b}(bg \to tH^-)$. Because of QCD backgrounds, only the low mass case gives a detectable signal over a non-negligible region of $(M_{A^0}, \tan\beta)$ [20].

At NLC energies, other than via bremsstrahlung and neutral pair production (this latter for $H^0A^0$ final states too [16]), MSSM Higgs bosons can be produced also via the fusion processes $e^+e^- \to \bar{\nu}_e\nu_e W^{\pm *}W^{\mp *}(e^+e^-Z^{0*}Z^{0*}) \to \bar{\nu}_e\nu_e(e^+e^-)h^0/H^0$ [21] and the charged pair production $e^+e^- \to \gamma^*, Z^{0*} \to H^+H^-$ [22]. The lightest $CP$-even Higgs boson $h^0$ can be detected over the whole MSSM parameter space, independently of the top and *squark* masses. Therefore, if the $h^0$ will not be found at the NLC, the MSSM is ruled out. If the $H^0$ and $A^0$ boson masses are less then $\approx 230$ GeV, there exists a very large area in the parameter space where all neutral Higgs bosons can be contemporaneously detected for $\sqrt{s}_{ee} = 500$ GeV [23]. A charged Higgs boson with $M_{H^\pm} < m_b + m_t$ mainly decays to $\nu_\tau\tau^+(\bar{\nu}_\tau\tau^-)$ and $c\bar{s}(\bar{c}s)$ pairs (with the leptonic mode dominating for tan$\beta > 1$). If kinematically allowed, a heavy $H^\pm$ decays via the top mode $H^\pm \to t\bar{b}(\bar{t}b)$ (and in some part of the parameter space also to $W^\pm h^0$). In both cases the signature is a cascade with a $\tau$ or a $b$ in the final state: therefore, an extremely good mass resolution is crucial in order to reduce the backgrounds from top and boson pair production. For an intermediate $H^\pm$, if tan$\beta > 1$, a possible signature is an apparent breaking of the $\tau$ vs $\mu/e$ universality. At higher $e^+e^-$ energies, such as $\sqrt{s}_{ee} = 1$–2 TeV, fusion mechanisms become dominant over other production processes [15,24].

The conversion of $e^+e^-$ NLC's into $\gamma\gamma$ and/or $e\gamma$ colliders, by photons generated via Compton back scattering of laser light, provides new possibilities of detecting and studying Higgs bosons [25]. For the MSSM, at a NLC with $\sqrt{s}_{ee} = 500$ GeV, $\gamma\gamma \to \Phi^0$ reactions are important in searching for heavy $H^0$ and $A^0$ bosons: they can be detected up to mass values of $\approx 0.8\sqrt{s}_{ee}$, for moderate tan$\beta$ and if a luminosity of 20 fb$^{-1}$, or more, can be achieved [26]. For the $H^0$, the channels $H^0 \to h^0h^0$, if $M_{H^0} \lesssim 2m_t$, and $H^0 \to t\bar{t}$, for $M_{H^0} \gtrsim 2m_t$, appear more interesting than the decays $H^0 \to b\bar{b}$ and $H^0 \to Z^0Z^0$. For the $A^0$, the feasible reactions are $\gamma\gamma \to A^0 \to Z^0h^0/b\bar{b}$, if $M_{A^0} \lesssim 2m_t$, and $\gamma\gamma \to A^0 \to t\bar{t}$, if $M_{A^0} \gtrsim 2m_t$. If tan$\beta \lesssim 20$, only the $b\bar{b}$ channel is useful for the $A^0$, with[6] $M_{A^0} \lesssim 250$ GeV. Recently, it has been shown that the intermediate mass $H^+H^-$ pair production via $\gamma\gamma$ fusion is greater (e.g., at least by a factor 2 at $\sqrt{s}_{ee} = 500$ GeV) than the corresponding $e^+e^-$ mode, and charged Higgs bosons can be detected using the three decay modes $\nu_\tau\tau^+\bar{\nu}_\tau\tau^-$, $c\bar{s}\bar{c}s$, and $c\bar{s}\bar{\nu}_\tau\tau^- + \nu_\tau\tau^+\bar{c}s$ in a complementary way in order to cover all the intermediate mass region of $H^\pm$ [27]. The $e\gamma$ option at NLC's is quite interesting in studying MSSM Higgs boson production via the processes $e^-\gamma \to \nu_eW^-\Phi^0$, $e^-\gamma \to \nu_eH^-\Phi^0$, and $e^-\gamma \to e^-H^+H^-$, in the intermediate mass range of $M_{A^0}$ and for a large choice of tan$\beta$'s [28].

The option of $ep$ colliders in detecting and studying MSSM Higgs bosons has been only marginally exploited, so far, with respect to the possibilities of $pp$ and $e^+e^-$ accelerators. The only presently operating $ep$ high energy machine is DESY HERA [29], which, however, has been primarily designed for providing accurate data on the proton structure functions in the small-$x$ region, more than being devoted to Higgs boson searches, which are almost impossible even for the more favorable cases of $A^0$ and $H^\pm$ production [30]. In fact, most of these searches rely on very special conditions, which seem to be excluded by recent limits on Higgs boson and top quark masses: e.g., very high tan$\beta$ ($\approx 40$) in order to detect neutral Higgs bosons $\Phi^0$ via $Z^0Z^0$ and $\gamma\gamma$ fusion processes [31], or very light charged Higgs bosons and/or

[3]Since the most part of the results on Higgs boson searches at the Superconducting Super Collider (SSC) can be transposed to the LHC, in the following we will arbitrarily confuse the two bibliographies on this argument, even though we know that the SSC project has been definitely set aside.

[4]For the *top* squark mass $m_{\tilde{t}} = 1$ TeV and all gaugino masses greater than 200 GeV.

[5]If the higher luminosity and a large number of tracks per event can successfully be dealt with.

[6]Since the $h^0$ mass never becomes large, the only important channel is $\gamma\gamma \to h^0 \to b\bar{b}$, allowing its detection for $M_{h^0} \gtrsim 60$ GeV ($M_{A^0} \gtrsim 70$ GeV).

top quark for $H^{\pm}$ production via $\gamma\gamma$ [32] and $\gamma g$ fusion [33]. Furthermore, the $H^{\pm}$-production mechanism via bremsstrahlung off heavy quarks $\gamma q \to q' H^{\pm}$ suffers from a strong Cabibbo-Kobayashi-Maskawa or $O(m_q/M_{W^{\pm}})$ suppression (where $q$ is the emitting initial light quark) [34]. Finally, the production of neutral MSSM Higgs bosons through bremsstrahlung off $b$ quarks, exploited in Ref. [35], can hardly be useful, since it depends not only on a good $b$ and/or heavy lepton tagging, but also on the fact that only large $\tan\beta$ ($\approx 20$) and Higgs boson

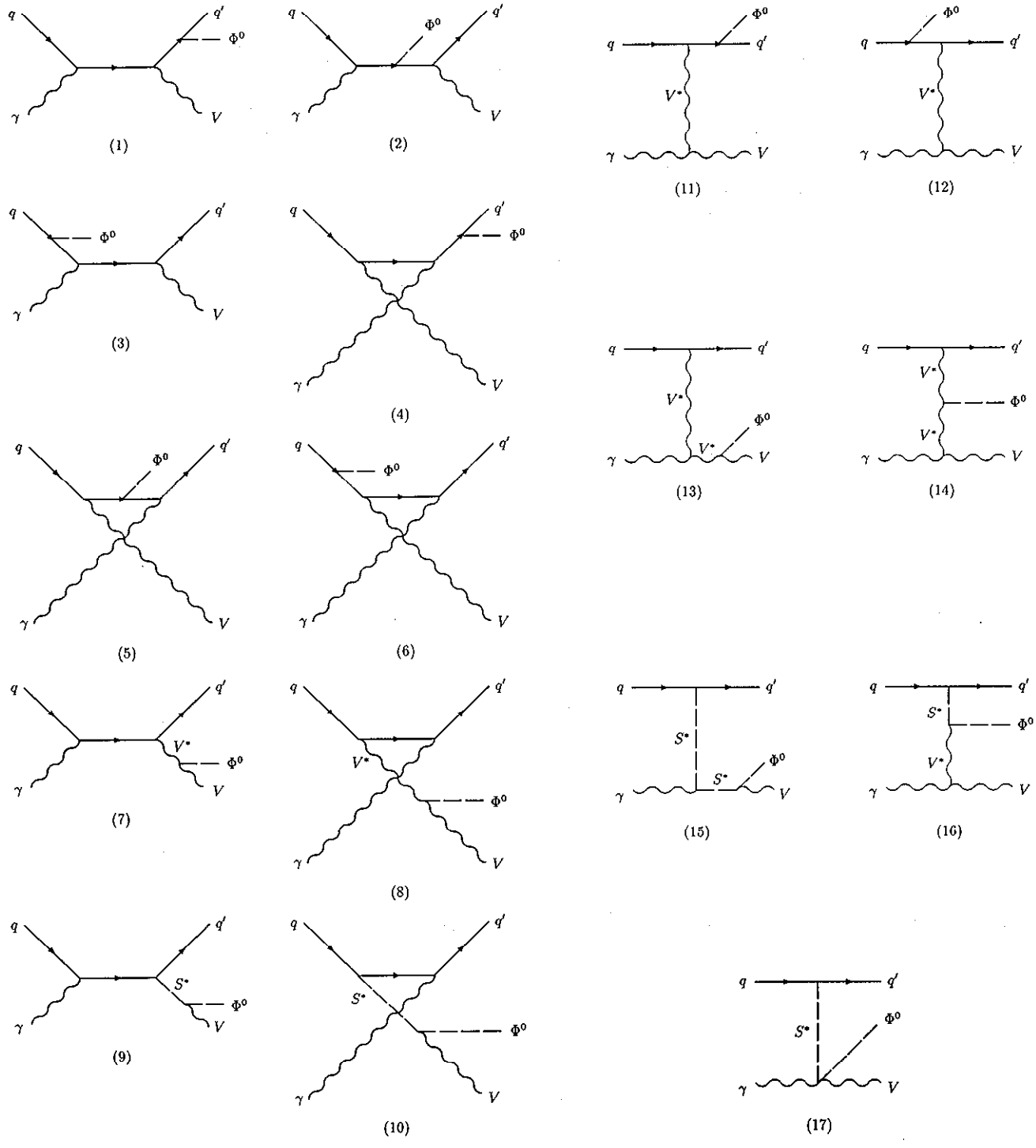


FIG. 1. Feynman diagrams contributing in the lowest order to $q\gamma \to q' V \Phi^0$, where $q(q')$ represents a quark, $V(V^*)$ an external (internal) vector boson, $S^*$ an internal scalar Higgs boson, and $\Phi^0$ one of the neutral MSSM Higgs bosons, in the unitary gauge. For the possible combinations of $(q, q', V, V^*, S^*, \Phi^0)$ and the corresponding nonvanishing graphs, see the text.

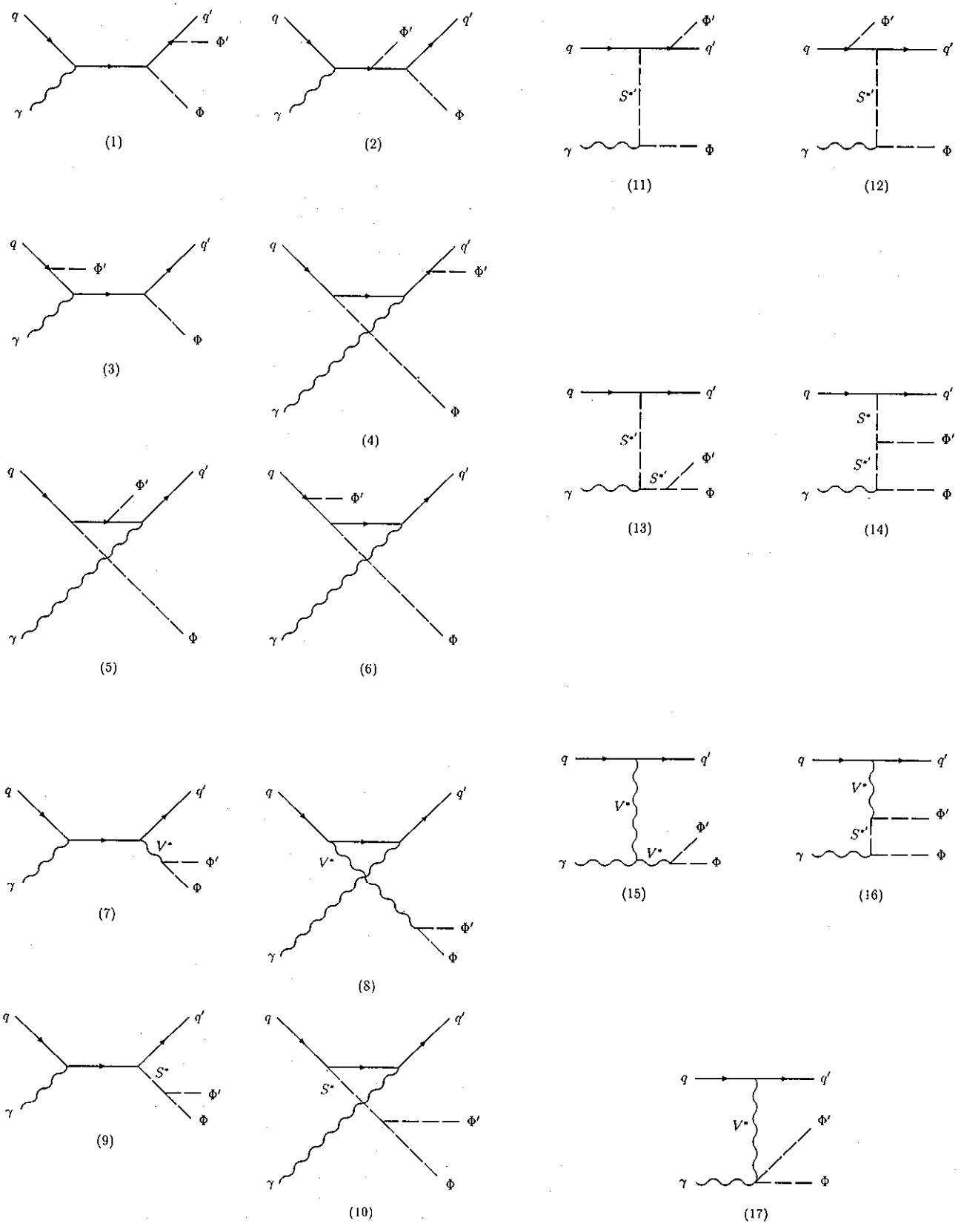


FIG. 2. Feynman diagrams contributing in the lowest order to $q\gamma \to q'\Phi\Phi'$, where $q(q')$ represents a quark, $V^*$ an internal vector boson, $S^*$ and $S^{*'}$ internal scalar Higgs bosons, and $\Phi$ and $\Phi'$ both neutral and charged MSSM Higgs bosons, in the unitary gauge. For the possible combinations of $(q, q', V^*, S^*, S^{*'}, \Phi, \Phi')$ and the corresponding nonvanishing graphs, see the text.

masses $M_{\Phi^0} \lesssim 90$ GeV can give detectable signals.[7]

In the future, another *ep* collider is contemplated to be operating, the CERN LEP⊗LHC machine, obtainable by combining an electron or positron beam of LEP II and a proton beam of the LHC [9,36]. The detailed studies on the detectability of an intermediate mass SM Higgs boson $\phi$ at such a machine presented in Ref. [37] (using $W^{\pm}W^{\mp}$ and $Z^0Z^0$ fusion processes [34,30,38,39], with $\phi$ decaying to $b\bar{b}$) can be transposed to the case of $CP$-even neutral MSSM Higgs bosons, but increasing the requirements on luminosity and/or on $b$-tagging identification, due to the smaller $H^0$ and $h^0$ cross sections with respect to the SM case. Charged Higgs bosons can be detected at LEP⊗LHC energies via the decay $t(\bar{t}) \to H^+b(H^-\bar{b})$, if $M_{H^{\pm}} \lesssim m_t - m_b$, while for $M_{H^{\pm}} \gtrsim m_t - m_b$, good sources of $H^{\pm}$ bosons are the photoproduction $\gamma b \to H^-t$ (through bremsstrahlung photons) and the $W^{\pm}$ mediated process $e^-b \to \nu_e H^-b$, studied in Ref. [40].

Concerning photon-initiated processes, only recently has the possibility of resorting to back-scattered laser $\gamma$'s, also at the CERN *ep* collider [41], been suggested. This option has been applied to the case of SM Higgs boson production but, obviously, it could turn out to be useful for MSSM Higgs bosons also.

It is the purpose of this paper to study at the LEP⊗LHC *ep* collider the reactions

$$q\gamma \to q'W^{\pm}\Phi^0, \tag{2}$$
$$q\gamma \to qZ^0\Phi^0, \tag{3}$$
$$q\gamma \to q'H^{\pm}\Phi^0, \tag{4}$$
$$q\gamma \to q\Phi^0\Phi^{0'}, \tag{5}$$
$$q\gamma \to qH^+H^-, \tag{6}$$
$$g\gamma \to q\bar{q}'H^{\pm}, \tag{7}$$
$$g\gamma \to q\bar{q}\Phi^0, \tag{8}$$

where $\Phi^{0(\prime)} = H^0$, $h^0$, and $A^0$, in the intermediate mass range of $A^0$, for all possible (anti)flavors of the (anti)quarks $q(q')$, using laser back-scattered photons. We discuss their relevance for the detection of the MSSM Higgs bosons and the study of their parameters, assuming $b$-tagging identification.

We did not study the processes

$$q\gamma \to qW^{\pm}H^{\mp}, \tag{9}$$

$$q\gamma \to q'Z^0H^{\pm}, \tag{10}$$

since here the MSSM Higgs bosons directly couple to the quark line in each Feynman diagram at tree level, so we expect that they are suppressed through the Yukawa coupling by the hadron structure functions, with respect to processes (2)–(8), where $\Phi^0$ and $H^{\pm}$ also couple to the vector bosons $\gamma$, $Z^0$, and $W^{\pm}$ [see diagrams (7), (8), (13), (14) of Fig. 1 and diagrams (7), (8), and (15)–(17) of Fig. 2].

[7]Region that can be more easily covered by LEP II.

There are at least two important motivations for studying processes (2)–(8), and at the LEP⊗LHC collider. First, as already pointed out in paper I of this study [42], the CERN *ep* option could be operating before any NLC, so it would constitute the first TeV energy environment partially free from the enormous background arising from QCD processes (typical of the purely hadron colliders), which prevents the possibility of detailed studies of the various parameters of an intermediate mass Higgs boson. Second, even in the case that LEP II and LHC can together cover all the parameter space ($M_{A^0}$, $\tan\beta$), nevertheless, processes (2)–(8) offer the opportunity for studying a large variety of MSSM interactions involving Higgs bosons: in fact, all the vertices displayed in Table X–XII occur. Moreover, the additional heavy particles $t(\bar{t})$, $W^{\pm}$, $Z^0$, and the second Higgs boson can be used for tagging purposes, increasing the signal versus background ratio.

In Ref. [42] we carried out a very similar analysis for the case of the SM. The encouraging results we have found there induced us to investigate if possibilities of Higgs boson detection and study also exist within the MSSM.

The plan of the present paper is as follows. In Sec. II we give some details of the calculation and of the parameters of the MSSM we have used, Sec. III is devoted to the presentation of the results while the conclusions are in Sec. IV. Finally, in the Appendix, we give the tree-level helicity amplitudes for processes (2)–(8).

## CALCULATION

In the unitary gauge the Feynman diagrams which enter in describing reactions (2)–(8) at tree level are shown in Figs. 1, 2, and 3. For the various possible combinations of $(q, q', V, V^*, S^*, \Phi^0)$ in Fig. 1, $(q, q', V^*, S^*, S^{*'}, \Phi, \Phi')$ in Fig. 2, and $(q, q', S^*, \Phi)$ in Fig. 3, see details in the Appendix. All quarks have been considered massive, so diagrams with a direct coupling of $\Phi^0/H^{\pm}$ to fermion lines have been computed for each combination of flavors.

The matrix elements have been evaluated by means of the spinor techniques of Refs. [43,44] and the FORTRAN codes have been compared with the corresponding ones implemented by the method of Ref. [45]. The amplitudes have been tested for gauge invariance, and it has been also verified that, with appropriate couplings, hadronic distributions, and luminosity function of photons, our results for the processes $q\gamma \to q'W^{\pm}\Phi^0$, $g\gamma \to q\bar{q}\Phi^0$, and $g\gamma \to t\bar{b}H^-$ reproduce those of Ref. [41] (for a SM Higgs boson), of Ref. [35] and of Ref. [33], respectively. Furthermore, since a simple adaptation of the formulas given in the Appendix (by changing photon couplings from quarks into leptons and setting the quark masses equal to zero) allows us to reproduce the computations of Ref. [28], we have checked, where possible, our helicity amplitudes also in these limits.

As proton structure functions we adopted the recent set Martin-Roberts-Stirling set A [MRS(A)] [46] (differ-

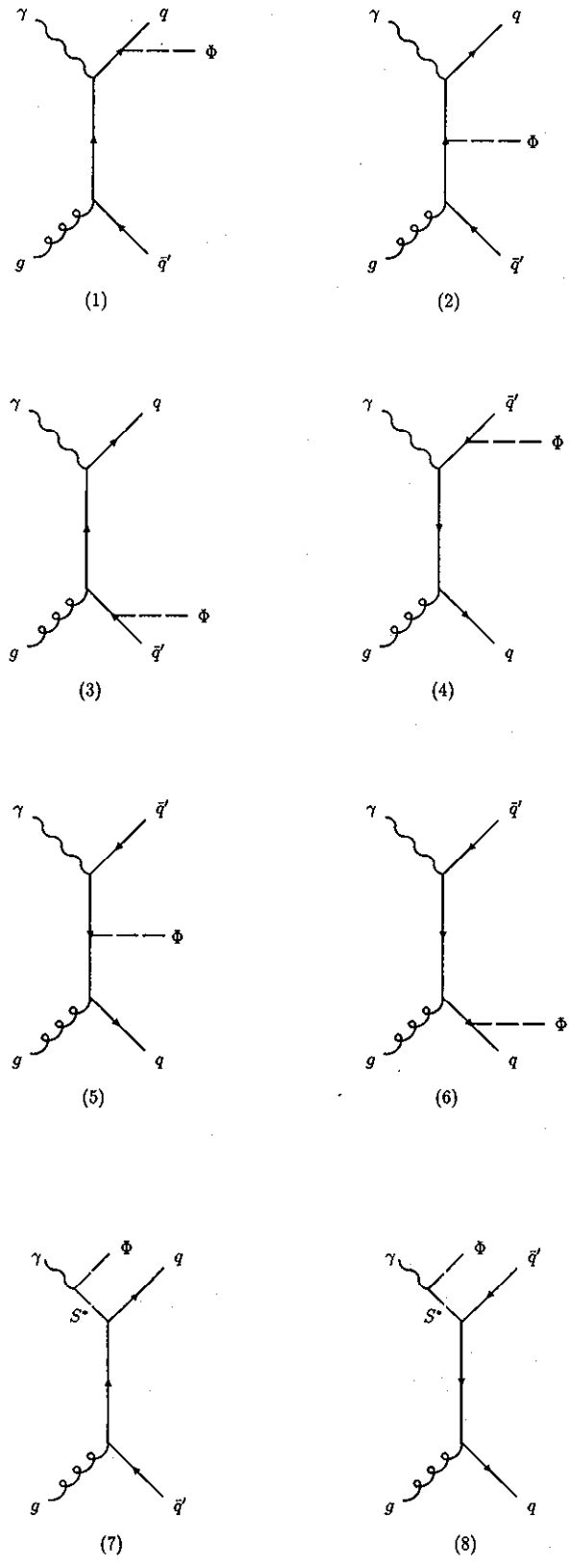


FIG. 3. Feynman diagrams contributing in the lowest order to $g\gamma \to q\bar{q}'\Phi$, where $q(q')$ represents a quark, $S^*$ an internal scalar Higgs boson, and $\Phi$ both neutral and charged MSSM Higgs bosons, in the unitary gauge. For the possible combinations of $(q, q', S^*, \Phi)$ and the corresponding nonvanishing graphs, see the text.

ently from the case of Ref. [42], where the set Harriman-MRS set B (HMRSB) was used [47]), fixing the $\mu$ scale equal to the center-of-mass energy (c.m.) at parton level (i.e., $\mu = \sqrt{\hat{s}}_{q(g)\gamma}$). The strong coupling constant $\alpha_s$, which appears in the gluon initiated processes, has been evaluated at next-to-leading order, with $\Lambda^4_{\rm QCD_{\overline{MS}}} = 230$ MeV, where $\overline{\rm MS}$ denotes the modified minimal subtraction scheme, and a scale $\mu$ equal to the one used for the proton structure functions, and consistent with the quark flavor entering in the partonic subprocess. We are confident that changing the energy scale and/or the distribution functions choice should not affect our results by more than a factor of 2.

As energy spectrum of the back-scattered photon we have used here the same one adopted in paper I. The same holds for the value of the luminosity we chose as well as for the computational procedure we adopted in evaluating the MSSM cross sections. Therefore, for all details and formulas we refer the reader to Ref. [42].

Within the MSSM, in order to simplify the discussion, we assume an universal soft supersymmetry-breaking mass [48,49]

$$m_Q^2 = m_U^2 = m_D^2 = m_{\tilde{q}}^2 , \tag{11}$$

and a negligible mixing in the *top* squark and *bottom* squark mass matrices

$$A_t = A_b = \mu = 0 . \tag{12}$$

If we also neglect the *bottom* mass in the formulas of Refs. [48,49], the one-loop corrected masses of the MSSM neutral $CP$-even Higgs bosons can be expressed in terms of a single parameter $\epsilon$ [50], given by

$$\epsilon = \frac{3e^2}{8\pi^2 M_{W^\pm}^2 \sin\theta_W} m_t^4 \ln\left(1 + \frac{m_{\tilde{q}}^2}{m_t^2}\right) . \tag{13}$$

Diagonalization of the mass squared matrix leads to the expressions[8]

$$\begin{aligned} M^2_{h^0,H^0} = \frac{1}{2}[M^2_{A^0} + M^2_{Z^0} + \epsilon/s^2_\beta] \\ \pm\{[(M^2_{A^0} - M^2_{Z^0})c_{2\beta} + \epsilon/s^2_\beta]^2 \\ + (M^2_{A^0} + M^2_{Z^0})^2 s^2_{2\beta}\}^{1/2} , \end{aligned} \tag{14}$$

while the mixing angle $\alpha$ in the $CP$-even sector is defined at one loop by

$$t_{2\alpha} = \frac{(M^2_{A^0} + M^2_{Z^0})s_{2\beta}}{(M^2_{A^0} - M^2_{Z^0})c_{2\beta} + \epsilon/s^2_\beta} , \quad -\frac{\pi}{2} < \alpha \le 0 . \tag{15}$$

For the MSSM charged Higgs boson masses we have maintained the tree-level relations

$$M^2_{H^\pm} = M^2_{A^0} + M^2_{W^\pm} , \tag{16}$$

[8]Throughout this paper we use the notations $s_x = \sin(x)$, $c_x = \cos(x)$, $t_x = \tan(x)$ (with $x = \alpha, \beta, 2\alpha$, and $2\beta$), $s_{\alpha\beta} = \sin(\beta + \alpha)$, $c_{\alpha\beta} = \cos(\beta + \alpha)$, $s_{\beta\alpha} = \sin(\beta - \alpha)$, and $c_{\beta\alpha} = \cos(\beta - \alpha)$.

since the one-loop corrections are quite small if compared with the corresponding ones for neutral Higgs bosons [49].

Concerning the numerical part of our work, we have used for the electromagnetic coupling constant, the Weinberg angle, the masses and the widths of fermions and gauge bosons the same values adopted in Ref. [42], apart from the top width, which has now been computed (at tree level) within the MSSM, using the expressions [51]

$$\frac{\Gamma(t\to bH^+)}{\Gamma(t\to bW^+)}=\frac{\lambda(H^2_{H^\pm},m_b^2,m_t^2)^{1/2}}{\lambda(M^2_{W^\pm},m_b^2,m_t^2)^{1/2}}\frac{(m_t^2+m_b^2-M^2_{H^\pm})(m_t^2t_\beta^{-2}+m_b^2t_\beta^2)+4m_t^2m_b^2}{M^2_{W^\pm}(m_t^2+m_b^2-2M^2_{W^\pm})+(m_t^2-m_b^2)^2}, \tag{17}$$

and [52]

$$\Gamma(t\to bW^+)=|V_{tb}|^2\frac{G_Fm_t}{8\sqrt{2}\pi}\lambda(M^2_{W^\pm},m_b^2,m_t^2)^{1/2}\times\left\{\left[1-\left(\frac{m_b}{m_t}\right)^2\right]^2+\left[1+\left(\frac{m_b}{m_t}\right)^2\right]\left(\frac{M_{W^\pm}}{m_t}\right)^2-2\left(\frac{M_{W^\pm}}{m_t}\right)^4\right\}, \tag{18}$$

where $V_{tb}$ is the Cabibbo-Kobayashi-Maskawa mixing term (here set equal to 1), $G_F=\sqrt{2}g^2/8M^2_{W^\pm}$ the electroweak Fermi constant, $g=e/s_W$ with $-e$ the electron charge, and $\lambda^{1/2}$ the usual kinematic factor

$$\lambda(M_a,M_b,M_c)^{1/2}=[M_a^2+M_b^2+M_c^2-2M_aM_b-2M_aM_c-2M_bM_c]^{1/2}. \tag{19}$$

The widths of the MSSM Higgs bosons have been evaluated for the same MSSM parameters we adopted in the cross section analysis: for the numerical values as for further details on their computation we refer to [53].

Finally, the universal supersymmetry-breaking squark mass has been fixed in the numerical analysis to the value $m_{\tilde{q}}=1$ TeV, and at the same time, for simplicity, we have ignored the presence of not-Higgs supersymmetric particles (i.e., squarks, sleptons, gauginos, higgsinos).

We have analyzed processes (2)–(8) in the mass range 60 GeV$\lesssim M_{A^0}\lesssim$ 140 GeV, with $\tan\beta=1.5$, 30, at the $ep$ c.m. energy $\sqrt{s_{ep}}=1.36$ TeV.

## RESULTS

As it is unpractical to cover all regions of the MSSM parameter space ($M_{A^0}$, $\tan\beta$) (for intermediate masses of the pseudoscalar Higgs boson), we have chosen here, as representative for $\tan\beta$, the two extreme values 1.5 and 30, whereas $M_{A^0}$ spans in the range 60 to 140 GeV. Also, due to the huge amount of computing time that otherwise would have been necessary, and contrary to the SM analysis of Ref. [42], we concentrate here only on the energy of the proposed CERN $ep$ collider ($\sqrt{s_{ep}}=1.36$ TeV) [9]. At this c.m. energy the cross sections (summed over all possible flavor combinations) for the processes

$$q\gamma\to q'W^\pm\Phi^0,\quad \Phi^0=H^0,h^0,A^0, \tag{20}$$

$$q\gamma\to qZ^0\Phi^0,\quad \Phi^0=H^0,h^0,A^0, \tag{21}$$

$$q\gamma\to q'H^\pm\Phi^0,\quad \Phi^0=H^0,h^0,A^0, \tag{22}$$

$$q\gamma\to q\Phi^0\Phi^{0'},\quad (\Phi^0,\Phi^{0'})=(H^0,A^0),(h^0,A^0), \tag{23}$$

$$q\gamma\to qH^+H^-, \tag{24}$$

$$g\gamma\to q\bar{q}'H^\pm, \tag{25}$$

$$g\gamma\to q\bar{q}\Phi^0,\quad \Phi^0=H^0,h^0,A^0, \tag{26}$$

are given in Tables I(a)–VII(b). Since the production rates for the reactions

$$q\gamma\to q\Phi^0\Phi^{0'},$$

$$(\Phi^0,\Phi^{0'})=(H^0,H^0),(H^0,h^0),(h^0,h^0),(A^0,A^0), \tag{27}$$

are generally[9] never larger than $\sim 10^{-2}$ fb and are beyond any experimental possibility of detection, we do not give their rates here and we will not consider them in the forthcoming analysis either.[10] Before proceeding further, a few comments are in order now, concerning the characteristics of the signals.

Process (20) gives quite large rates for the case $\Phi^0=H^0$ and not too large values of $M_{A^0}$ ($\lesssim 120$ GeV), both for $\tan\beta=1.5$ and $\tan\beta=30$, with the cross sections

[9] Apart from the cases $(h^0,h^0)$ and $(A^0,A^0)$ for $M_{A^0}=60$–80 GeV, with $\tan\beta=1.5$, 30, and 30, respectively, which can reach cross sections of $\sim 1$ fb.

[10] Also, in some instances, results given in Tables I(a)–VII(b) will be very small. Nevertheless, we present them with the purpose of comparison, in order to facilitate the discussion in terms of dependence on masses, couplings, etc.

TABLE I. Cross sections of the process $q\gamma \to q'W^{\pm}\Phi^0$, where $\Phi^0 = H^0, h^0, A^0$, at $\sqrt{s}_{ep} = 1.36$ TeV, for $M_{A^0} = 60, 80, 100, 120, 140$ GeV, with $\tan\beta = 1.5$ (a) and 30 (b). The MRS (A) structure functions are used. The errors are the statistical errors on the numerical calculation. Entries are in GeV for masses, and in fb for cross sections.

(a)
$\sigma(q\gamma \to q'W^{\pm}\Phi^0)$

| $M_{H^0}$ | $M_{h^0}$ | $M_{A^0}$ | $H^0$ | $h^0$ | $A^0$ |
|---|---|---|---|---|---|
| 144.4 | 56.0 | 60 | 7.582±0.024 | 37.30±0.16 | 0.25820±0.00090 |
| 150.7 | 63.7 | 80 | 5.767±0.019 | 36.76±0.19 | 0.18718±0.00058 |
| 159.3 | 70.6 | 100 | 3.986±0.011 | 36.80±0.17 | 0.13096±0.00043 |
| 170.1 | 76.4 | 120 | 2.5569±0.0069 | 37.02±0.14 | 0.09185±0.00030 |
| 182.9 | 80.9 | 140 | 1.5431±0.0045 | 37.44±0.14 | 0.06441±0.00020 |
| | | $\sqrt{s} = 1.36$ TeV | $\tan\beta = 1.5$ | | MRS (A) |

(b)
$\sigma(q\gamma \to q'W^{\pm}\Phi^0)$

| $M_{H^0}$ | $M_{h^0}$ | $M_{A^0}$ | $H^0$ | $h^0$ | $A^0$ |
|---|---|---|---|---|---|
| 129.2 | 59.9 | 60 | 24.060±0.074 | 0.8430±0.0018 | 1.5041±0.0044 |
| 129.2 | 79.9 | 80 | 23.959±0.075 | 0.6993±0.0015 | 0.9990±0.0026 |
| 129.4 | 99.7 | 100 | 23.692±0.074 | 0.8049±0.0019 | 0.6780±0.0016 |
| 130.0 | 119.0 | 120 | 21.485±0.067 | 2.9355±0.0087 | 0.4636±0.0012 |
| 140.9 | 128.1 | 140 | 1.4487±0.0042 | 22.964±0.070 | 0.31958±0.00076 |
| | | $\sqrt{s} = 1.36$ TeV | $\tan\beta = 30$ | | MRS (A) |

corresponding to the last case being larger. Significantly large numbers occur also in the case $\Phi^0 = h^0$, more at small than at large $\tan\beta$'s. Phase space effects due to the increase of $M_{H^0}$ and $M_{h^0}$ lower down the cross sections, whereas the strong change of trend at large $\tan\beta$'s and $M_{A^0} \approx 120$–$140$ GeV is due to the sudden steep decrease of the $H^0W^+W^-$ coupling (proportional to $c_{\beta\alpha}$), and to the corresponding increase of the $h^0W^+W^-$ one (proportional to $s_{\beta\alpha}$). Higgs boson bremsstrahlungs diagrams (numbers 1–6 in Fig. 1) are in fact drastically suppressed because of the Yukawa coupling $\Phi^0 q\bar{q}$, proportional to $m_q$, since $q$ (due to the partonic distributions) is most of the times a light quark. Because of this, and since the $A^0$ does not couple at tree level to the $W^{\pm}$'s, the case $\Phi^0 = A^0$ generally gives much smaller rates. Only the case $\tan\beta = 30$ (i.e., large $\Phi^0 D\bar{D}$ coupling to down-type quarks $D$), for small enough phase space suppression (i.e., if $M_{A^0} \approx 60$ GeV), can give cross sections of $\sim 1$ fb.

Same considerations as the above mentioned apply to the case of reaction (21), even though the suppressed

TABLE II. Cross sections of the processes $q\gamma \to qZ^0\Phi^0$, where $\Phi^0 = H^0, h^0, A^0$, at $\sqrt{s}_{ep} = 1.36$ TeV, for $M_{A^0} = 60, 80, 100, 120, 140$ GeV, with $\tan\beta = 1.5$ (a) and 30 (b). The MRS (A) structure functions are used. The errors are the statistical errors on the numerical calculation. Entries are in GeV for masses, and in fb for cross sections.

(a)
$\sigma(q\gamma \to qZ^0\Phi^0)$

| $M_{H^0}$ | $M_{h^0}$ | $M_{A^0}$ | $H^0$ | $h^0$ | $A^0$ |
|---|---|---|---|---|---|
| 144.4 | 56.0 | 60 | 0.1913±0.0031 | 4.877±0.050 | $(7.962 \pm 0.023) \times 10^{-3}$ |
| 150.7 | 63.7 | 80 | 0.1283±0.0014 | 3.941±0.045 | $(5.186 \pm 0.015) \times 10^{-3}$ |
| 159.3 | 70.6 | 100 | 0.0803±0.0011 | 3.260±0.065 | $(3.551 \pm 0.010) \times 10^{-3}$ |
| 170.1 | 76.4 | 120 | 0.0419±0.0014 | 2.998±0.037 | $(2.4628 \pm 0.0078) \times 10^{-3}$ |
| 182.9 | 80.9 | 140 | 0.02421±0.00028 | 2.705±0.037 | $(1.7317 \pm 0.0051) \times 10^{-3}$ |
| | | $\sqrt{s} = 1.36$ TeV | $\tan\beta = 1.5$ | | MRS (A) |

(b)
$\sigma(q\gamma \to qZ^0\Phi^0)$

| $M_{H^0}$ | $M_{h^0}$ | $M_{A^0}$ | $H^0$ | $h^0$ | $A^0$ |
|---|---|---|---|---|---|
| 129.2 | 59.9 | 60 | 0.7443±0.0085 | 1.3557±0.0047 | 2.2500±0.0080 |
| 129.2 | 79.9 | 80 | 0.7406±0.0073 | 0.9509±0.0032 | 1.5374±0.0052 |
| 129.4 | 99.7 | 100 | 0.7474±0.0078 | 0.6819±0.0023 | 1.0753±0.0040 |
| 130.0 | 119.0 | 120 | 0.677±0.015 | 0.5162±0.0022 | 0.7622±0.0031 |
| 140.9 | 128.1 | 140 | 0.3412±0.0011 | 0.770±0.017 | 0.5376±0.0018 |
| | | $\sqrt{s} = 1.36$ TeV | $\tan\beta = 30$ | | MRS (A) |

TABLE III. Cross sections of the processes $q\gamma \to q' H^{\pm}\Phi^0$, where $\Phi^0 = H^0, h^0, A^0$, at $\sqrt{s}_{ep} = 1.36$ TeV, for $M_{A^0} = 60, 80, 100, 120, 140$ GeV, with $\tan\beta = 1.5$ (a) and 30 (b). The MRS (A) structure functions are used. The errors are the statistical errors on the numerical calculation. Entries are in GeV for masses, and in fb for cross sections.

(a)

| $M_{H^0}$ | $M_{h^0}$ | $M_{A^0}$ | $M_{H^\pm}$ | $\sigma(q\gamma \to q' H^{\pm}\Phi^0)$ $H^0$ | $h^0$ | $A^0$ |
|---|---|---|---|---|---|---|
| 144.4 | 56.0 | 60 | 100.0 | 0.3621±0.0019 | 1.1599±0.0085 | 2.834±0.021 |
| 150.7 | 63.7 | 80 | 113.1 | 0.2683±0.0017 | 0.5857±0.0037 | 1.3684±0.0072 |
| 159.3 | 70.6 | 100 | 128.1 | 0.1944±0.0011 | 0.2866±0.0021 | 0.6745±0.0037 |
| 170.1 | 76.4 | 120 | 144.2 | 0.1334±0.00081 | 0.1352±0.0013 | 0.3518±0.0021 |
| 182.9 | 80.9 | 140 | 161.2 | 0.08182±0.00059 | 0.06572±0.00031 | 0.1858±0.0011 |
| | | $\sqrt{s} = 1.36$ TeV | | $\tan\beta = 1.5$ | | MRS (A) |

(b)

| $M_{H^0}$ | $M_{H^0}$ | $M_{A^0}$ | $M_{H^\pm}$ | $\sigma(q\gamma \to q' H^{\pm}\Phi^0)$ $H^0$ | $h^0$ | $A^0$ |
|---|---|---|---|---|---|---|
| 129.2 | 59.9 | 60 | 100.0 | $(6.833 \pm 0.019) \times 10^{-3}$ | 2.8210±0.019 | 2.833±0.020 |
| 129.2 | 79.9 | 80 | 113.1 | $(6.527 \pm 0.029) \times 10^{-3}$ | 1.3660±0.0081 | 1.3697±0.0072 |
| 129.4 | 99.7 | 100 | 128.1 | $(8.344 \pm 0.044) \times 10^{-3}$ | 0.6732±0.0056 | 0.6758±0.0037 |
| 130.0 | 119.0 | 120 | 144.2 | $(31.52 \pm 0.24) \times 10^{-3}$ | 0.3224±0.0019 | 0.3523±0.0021 |
| 140.9 | 128.1 | 140 | 161.2 | $(171.3 \pm 1.0) \times 10^{-3}$ | 0.015369±0.000073 | 0.1860±0.0011 |
| | | $\sqrt{s} = 1.36$ TeV | | $\tan\beta = 30$ | | MRS (A) |

$\Phi^0 Z^0 Z^0$ couplings (with respect to the case $\Phi^0 W^+ W^-$, being $\Phi^0 = H^0, h^0$) yield contributions which are in general an order of magnitude smaller than in the previous case. At $\tan\beta = 1.5$ only the $h^0$ seems to be interesting, whereas at $\tan\beta = 30$ both the $H^0$ and the $h^0$ show negligible numbers. Finally, graphs with Higgs-strahlungs off $b$ quarks contribute to keep the rates for the $A^0$ at $\tan\beta = 30$ at the level of $\sim 1$ fb, if $M_{A^0}$ is not too large, whereas at $\tan\beta = 1.5$ numbers are completely negligible.

The coupling of the $A^0$ to the vertices $\Phi^0 W^{\pm} H^{\mp}(\gamma)$ (see Table X in the Appendix) does not suffer from angular factor suppression (there is no dependence on $\alpha$

TABLE IV. Cross sections of the processes $q\gamma \to q\Phi^0\Phi^{0'}$, where $(\Phi^0, \Phi^{0'}) = (H^0, A^0), (h^0, A^0)$, at $\sqrt{s}_{ep} = 1.36$ TeV, for $M_{A^0} = 60, 80, 100, 120, 140$ GeV, with $\tan\beta = 1.5$ (a) and 30 (b). The MRS (A) structure functions are used. The errors are the statistical errors on the numerical calculation. Entries are in GeV for masses, and in fb for cross sections.

(a)

| $M_{H^0}$ | $M_{h^0}$ | $M_{A^0}$ | $\sigma(q\gamma \to q\Phi^0\Phi^{0'})$ $H^0A^0$ | $h^0A^0$ |
|---|---|---|---|---|
| 144.4 | 56.0 | 60 | 0.1468±0.0023 | 1.0889±0.0092 |
| 150.7 | 63.7 | 80 | 0.1004±0.0014 | 0.3226±0.0041 |
| 159.3 | 70.6 | 100 | 0.0715±0.0013 | 0.1183±0.0018 |
| 170.1 | 76.4 | 120 | 0.0409±0.00056 | 0.0437±0.00075 |
| 182.9 | 80.9 | 140 | 0.02656±0.00049 | 0.0203±0.00025 |
| $\sqrt{s} = 1.36$ TeV | | | $\tan\beta = 1.5$ | MRS (A) |

(b)

| $M_{H^0}$ | $M_{h^0}$ | $M_{A^0}$ | $\sigma(q\gamma \to q\Phi^0\Phi^{0'})$ $H^0A^0$ | $h^0A^0$ |
|---|---|---|---|---|
| 129.2 | 59.9 | 60 | $(6.072 \pm 0.024) \times 10^{-3}$ | 4.002±0.039 |
| 129.2 | 79.9 | 80 | $(4.279 \pm 0.026) \times 10^{-3}$ | 1.1668±0.0098 |
| 129.4 | 99.7 | 100 | $(4.489 \pm 0.057) \times 10^{-3}$ | 0.4270±0.0038 |
| 130.0 | 119.0 | 120 | $(16.05 \pm 0.18) \times 10^{-3}$ | 0.1746±0.0021 |
| 140.9 | 128.1 | 140 | $(79.9 \pm 1.0) \times 10^{-3}$ | 0.00802±0.00013 |
| $\sqrt{s} = 1.36$ TeV | | | $\tan\beta = 30$ | MRS (A) |

TABLE V. Cross sections of the process $q\gamma \to qH^+H^-$, at $\sqrt{s}_{ep} = 1.36$ TeV, for $M_{A^0} = 60, 80, 100, 120, 140$ GeV, with $\tan\beta = 1.5$ (a) and 30 (b). The MRS (A) structure functions are used. The errors are the statistical errors on the numerical calculation. Entries are in GeV for masses, and in fb for cross sections.

(a)

| $M_{H^\pm}$ | $\sigma(q\gamma \to qH^+H^-)$ $H^+H^-$ | |
|---|---|---|
| 100.0 | 18.18±0.42 | |
| 113.1 | 10.96±0.16 | |
| 128.1 | 6.06±0.16 | |
| 144.2 | 2.991±0.064 | |
| 161.2 | 1.577±0.034 | |
| $\sqrt{s} = 1.36$ TeV | $\tan\beta = 1.5$ | MRS (A) |

(b)

| $M_{H^\pm}$ | $\sigma(q\gamma \to qH^+H^-)$ $H^+H^-$ | |
|---|---|---|
| 100.0 | 28.13±0.40 | |
| 113.1 | 16.52±0.21 | |
| 128.1 | 9.52±0.14 | |
| 144.2 | 4.244±0.056 | |
| 161.2 | 1.867±0.071 | |
| $\sqrt{s} = 1.36$ TeV | $\tan\beta = 30$ | MRS (A) |

TABLE VI. Cross sections of the process $g\gamma \to q\bar{q}'H^{\pm}$, at $\sqrt{s}_{ep} = 1.36$ TeV, for $M_{A^0} = 60, 80, 100, 120, 140$ GeV, with $\tan\beta = 1.5$ (a) and 30 (b). The MRS (A) structure functions are used. The errors are the statistical errors on the numerical calculation. Entries are in GeV for masses, and in fb for cross sections.

| | (a) $\sigma(g\gamma \to q\bar{q}'H^{\pm})$ | |
|---|---|---|
| $M_{H^{\pm}}$ | $H^{\pm}$ | |
| 100.0 | 367.3±2.7 | |
| 113.1 | 270.5±3.8 | |
| 128.1 | 174.3±1.0 | |
| 144.2 | 84.78±0.48 | |
| 161.2 | 22.78±0.15 | |
| $\sqrt{s} = 1.36$ TeV | $\tan\beta = 1.5$ | MRS (A) |
| | (b) $\sigma(g\gamma \to q\bar{q}'H^{\pm})$ | |
| $M_{H^{\pm}}$ | $H^{\pm}$ | |
| 100.0 | 621.7±4.8 | |
| 113.1 | 460.6±6.0 | |
| 128.1 | 291.9±1.7 | |
| 144.2 | 142.2±1.7 | |
| 161.2 | 40.65±0.31 | |
| $\sqrt{s} = 1.36$ TeV | $\tan\beta = 30$ | MRS (A) |

and $\beta$), whereas $H^0$'s and $h^0$'s do. Therefore, the rates for the $A^0$ in the case of reaction (22) are larger than the ones of the $CP$-even scalars, both a $\tan\beta = 1.5$ and $\tan\beta = 30$. This latter observation is always true apart from the case $\tan\beta = 30$ and $M_{A^0} \lesssim 120$ GeV, where numbers for the pseudoscalar and the light scalar are practically the same, as the value of $c_{\beta\alpha}$ approaches 1. This also proves that diagrams with $\Phi^0 H^+ H^-$ couplings (graphs 13–14 in Fig. 2, which are zero for $\Phi^0 = A^0$) do not count. The same can be affirmed for neutral Higgs boson bremsstrahlung diagrams, because they always occur in conjunction with a $H^{\pm}q\bar{q}'$ Yukawa coupling (see the practically unchanged rates for the $A^0$ at both values of $\tan\beta$).

The case $(\Phi^0, \Phi^{0'}) = (H^0, A^0)$ in process (23) is never interesting (and it has been shown for comparison purposes only, against the combination $h^0 A^0$). Due to the double Yukawa coupling, diagrams 1–6 in Fig. 2 essentially never enter. Diagrams 9–10 are strongly suppressed at $\tan\beta = 1.5$, whereas at $\tan\beta = 30$ they give a small contribution (because of the $A^0 D\bar{D}$ vertex). However, the largest rates come from diagrams 7–8, which are proportional to $s^2_{\beta\alpha}$ and $c^2_{\beta\alpha}$, for the $H^0$ and the $h^0$, respectively. As the second coupling is larger than the first one and $M_{H^0} > M_{h^0}$ in our range of interest, it is clear that $H^0$ rates are again smaller compared to the $h^0$ ones (especially at $\tan\beta = 30$).

Process (24) is one of those for which the production rates are bigger, if $M_{A^0}$ is not too large. The major partonic contributions here come from the subprocess with resonant top quarks (i.e., $b\gamma \to bH^+H^-$). Diagrams with $\gamma^*(Z^{0*})H^+H^-$ couplings (i.e., with a virtual photon or $Z^0$ splitting into $H^+H^-$ pairs) are dominant only in the other cases (for $q = u, d, s, c$). The increase of the rates with $\tan\beta$ is due to the larger contribution of graphs 8–10 and 13–14, which involve $\Phi^0 D\bar{D}$ couplings ($\Phi^0 = H^0$ and $h^0$).

For process (25), practically, the whole of the partonic contribution comes from the combination $g\gamma \to t\bar{b}H^+$+c.c., because of the $bt$ Yukawa couplings of the $H^{\pm}$ and because of the top resonance. Therefore, the increase of the rates with the increase of $\tan\beta$ in Tables VI(a) and VI(b) exclusively depends on and can be un-

TABLE VII. Cross sections of the processes $g\gamma \to q\bar{q}\Phi^0$, where $\Phi^0 = H^0, h^0, A^0$, at $\sqrt{s}_{ep} = 1.36$ TeV, for $M_{A^0} = 60, 80, 100, 120, 140$ GeV, with $\tan\beta = 1.5$ (a) and 30 (b). The MRS (A) structure functions are used. The errors are the statistical errors on the numerical calculation. Entries are in GeV for masses, and in fb for cross sections.

| | | | (a) $\sigma(g\gamma \to q\bar{q}\Phi^0)$ | | |
|---|---|---|---|---|---|
| $M_{H^0}$ | $M_{h^0}$ | $M_{A^0}$ | $H^0$ | $h^0$ | $A^0$ |
| 144.4 | 56.0 | 60 | 0.1914 ± 0.0047 | 2.1015 ± 0.0059 | 1.4169 ± 0.0041 |
| 150.7 | 63.7 | 80 | 0.1541 ± 0.0020 | 1.6574 ± 0.0051 | 0.6810 ± 0.0022 |
| 159.3 | 70.6 | 100 | 0.1174 ± 0.0029 | 1.3948 ± 0.0036 | 0.3640 ± 0.0019 |
| 170.1 | 76.4 | 120 | 0.0844 ± 0.0025 | 1.2121 ± 0.0030 | 0.2081 ± 0.0010 |
| 182.9 | 80.9 | 140 | 0.0588 ± 0.0014 | 1.1043 ± 0.0025 | 0.1253 ± 0.00092 |
| | | $\sqrt{s} = 1.36$ TeV | $\tan\beta = 1.5$ | | MRS (A) |
| | | | (b) $\sigma(g\gamma \to q\bar{q}\Phi^0)$ | | |
| $M_{H^0}$ | $M_{h^0}$ | $M_{A^0}$ | $H^0$ | $h^0$ | $A^0$ |
| 129.2 | 59.9 | 60 | 0.2743 ± 0.0010 | 428.3 ± 1.7 | 449.9 ± 1.6 |
| 129.2 | 79.9 | 80 | 0.3432 ± 0.0011 | 209.13 ± 0.83 | 218.87 ± 0.85 |
| 129.4 | 99.7 | 100 | 0.6488 ± 0.0020 | 115.30 ± 0.55 | 117.97 ± 0.53 |
| 130.0 | 119.0 | 120 | 8.649 ± 0.027 | 62.86 ± 0.28 | 67.66 ± 0.31 |
| 140.9 | 128.1 | 140 | 36.38 ± 0.17 | 4.514 ± 0.020 | 40.76 ± 0.19 |
| | | $\sqrt{s} = 1.36$ TeV | $\tan\beta = 30$ | | MRS (A) |

derstood in terms of the coupling $H^{\pm}tb$. Graphs with $\gamma H^+H^-$ vertices are generally suppressed in the $tbH^{\pm}$ case, and phase space effects act in such a way to strongly reduce the rates for increasing $M_{A^0}$ (because of the quite large value of $m_t$).

In case of process (26) we can greatly appreciate the benefits of $\Phi^0 D\bar{D}$ Yukawa couplings with large $\tan\beta$: in fact, all the flavors $\Phi^0 = H^0$, $h^0$, and $A^0$ have large cross sections at $\tan\beta = 30$. This happens especially for the pseudoscalar (it has a $\sim \tan\beta$ quark coupling) and the light scalar ($\sim s_\alpha/c_\beta$ quark coupling). The decrease of their rates with an increasing $M_{A^0}$ is due to a phase space effect in the former case, whereas in the latter also a reduction due to the diminishing of $s_\alpha$ occurs. Since the $H^0$ quark coupling is proportional to $c_\alpha/c_\beta$, in this case things proceed the other way round. In addition, the suppression due to phase space effects is small here, as $M_{H^0}$ varies by only $\approx 10$ GeV in the usual $M_{A^0}$ range, if $\tan\beta = 30$. At $\tan\beta = 1.5$ rates are generally much smaller, being noticeable only for $h^0$ (small mass and large $s_\alpha$).

The main lines of the analysis we will perform in order to select the signal events out of the backgrounds are the same ones already adopted for the SM case, in Ref. [42]. In order to maximize the event rates, we will consider the decay channels with highest branching ratio (BR). Therefore, we will look for the Higgs boson decay channel $\Phi^0 \to b\bar{b}$ for the neutral Higgs boson flavors $h^0$, $A^0$, and $H^0$, whereas, in case of charged Higgs bosons, we will concentrate on the decay $H^{\pm} \to \tau\nu_\tau$. We know that for $\tan\beta = 1.5(30)$ and 60 GeV$\leq M_{A^0} \leq$ 140 GeV ($M_{A^0} \approx 60$ GeV), corresponding to 145 GeV$\lesssim M_{H^0} \lesssim$ 180 GeV ($M_{H^0} \approx 129$ GeV), the BR's of the decay channels $H^0 \to W^{+*}W^{-*}(H^0 \to W^{+*}W^{-*})$ and, for $M_{H^0} \lesssim 150$ GeV, $H^0 \to h^0h^0(H^0 \to h^0h^0$ and $H^0 \to A^0A^0)$, are larger than $B(H^0 \to b\bar{b})$ [53]. Nevertheless, we concentrate here on the last decay only, for various reasons. In the case of $W^{+*}W^{-*}$ decays, we should first add, in any case, an additional reduction factor due to the $W^{\pm *}$ decay channels (that we should, in some way, identify). Second, we would end up considering signatures of the type $jj(Y)$, $(\tau\nu_\tau)(Y)$ or $(b\bar{b})(Y)$ (see later on), where $Y = 4j, 2j2l$, or $4l$, with the clear disadvantages of dealing either with a larger number of jets (for $Y = 4j, 2jl\nu_l$, which would have both a large QCD and combinatorial background) or with missing energy or momenta (for $Y = l\nu_l l\nu_l$, which would prevent from reconstructing Higgs boson peaks by means of invariant mass spectra). In the case of $h^0h^0$ and $A^0A^0$ decays, in order to keep high rates, we should consider the channels $h^0h^0, A^0A^0 \to 4b$, which would lead to the difficult requirement of recognizing with high efficiency at least four $b$'s in a single event. Whereas the decay $H^0 \to b\bar{b}$ implies that the only reduction factor is the $b\bar{b}$ BR, which ranges in the above interval of $M_{H^0}$, for $\tan\beta = 1.5(30)$, between $\approx 4(3)$ and $\approx 20(90)\%$ [53]. In the case of charged Higgs boson decays, if $\tan\beta = 1.5$ and $M_{H^{\pm}} \gtrsim 150$ GeV, the $tb$ channel has a BR larger than the one into $\tau\nu_\tau$ pairs. However, as $B(H^{\pm} \to tb)$ is not too drastically larger (so the loss of statistics is not substantial) and the decay chain $H^{\pm} \to tb \to b\bar{b}W^{\pm} + b\bar{b}H^{\pm}$ would lead to a more complicated final state with additional backgrounds, for the moment, we consider the $H^{\pm} \to \tau\nu_\tau$ channel only.

We will require hadronic decays of the massive vectors bosons ($W^{\pm}$ and $Z^0$) and, in order to select the $b\bar{b}$ Higgs boson decay out of the QCD background, we will assume excellent flavor identification of $b$ quarks [54], such that we can get rid of the non-$b$ multijet photoproduction, $W^{\pm}$+ jets and $Z^0$+ jets background events [41], and that a $M_{b\bar{b}}$ cut around the $\Phi^0$ masses (see later on) is sufficient in order to suppress the above processes in the case of $\gamma^*/g^* \to b\bar{b}$ splitting.

Therefore, we expect the following signatures:

$$q'W^{\pm}\Phi^0 \to (jj)(b\bar{b})X\,, \tag{28}$$

$$qZ^0\Phi^0 \to (jj)(b\bar{b})X\,, \tag{29}$$

$$q'H^{\pm}\Phi^0 \to (\tau\nu_\tau)(b\bar{b})X\,, \tag{30}$$

$$qH^0A^0, qh^0A^0 \to (b\bar{b})(b\bar{b})X\,, \tag{31}$$

$$qH^+H^- \to (\tau\nu_\tau)(\tau\nu_\tau)X\,, \tag{32}$$

$$q\bar{q}'H^{\pm} \to jj(\tau\nu_\tau)X \text{ (if } q\bar{q}' \neq t\bar{b})$$

$$\text{or } t\bar{b}(\tau\nu_\tau)X \to b\bar{b}(\tau\nu_\tau)X \text{ (if } q\bar{q}' = t\bar{b})\,, \tag{33}$$

$$q\bar{q}\Phi^0 \to (jj)(b\bar{b})X \text{ (if } q \neq b,t) \text{ or } (b\bar{b})(b\bar{b})X \text{ (if } q = b,t)\,, \tag{34}$$

where $X$ represents the untagged particles in the final states.

Concerning the expected backgrounds[11] to the above signatures, in case of neutral scalar production [i.e., Eqs. (28)–(31) and (34)] we have to consider the same processes already analyzed in Ref. [42] for the SM: i.e., $ep \to W^{\pm}Z^0X$, $ep \to \bar{t}bX \to b\bar{b}W^-X$, $ep \to t\bar{t}X \to b\bar{b}W^{\pm}X$, $ep \to Z^0Z^0X$, and $ep \to q\bar{q}Z^0$. In the case of double and single charged scalar production [i.e., Eqs. (32) and (33), respectively], we must add the reactions $ep \to W^+W^-X$ and $ep \to tbW^{\pm}X$. We also notice how the process $ep \to Z^0Z^0X$ is a background to $H^+H^-$ production when $Z^0Z^0 \to (\tau^+\tau^-)(\nu_\tau\bar{\nu}_\tau)$ and that the double and single top-resonant backgrounds $t\bar{t}X$ and $tbX$, as in the MSSM $t$ quarks can decay either to $bW^{\pm}$ or $bH^{\pm}$ pairs, are a potential background for $W^{\pm}\Phi^0X \to W^{\pm}(b\bar{b})X$, $H^{\pm}\Phi^0X \to H^{\pm}(b\bar{b})X$, and $t\bar{b}H^- + \bar{t}bH^+ \to b\bar{b}H^{\pm}X$.

In Table VIII(a) and VIII(b) we update the results given in [42] for the neutral scalar production back-

[11]These have been evaluated with the help of MADGRAPH and HELAS [55].

TABLE VIII. Production cross sections for the discrete and continuum background processes discussed in the text. Case (a) contains the cross sections which do not have dependence on the MSSM parameters, whereas (b) shows the case in which resonant $t$ quarks introduce such a dependence through $\Gamma_t^{\rm MSSM}$. In (b) the five entries for each process correspond to the five different values of $M_{A^0} = 60$, 80, 100, 120, and 140 GeV. Numbers in brackets are for the case $\tan\beta = 30$. The MRS (A) structure functions are used. The errors are the statistical errors on the numerical calculation. Entries are in GeV for masses, and in fb for cross sections.

(a)

| Background | $\sigma$ |
|---|---|
| $ep \to W^\pm Z^0 X$ | $219.8 \pm 3.2$ |
| $ep \to Z^0 Z^0 X$ | $10.98 \pm 0.60$ |
| $ep \to q\bar{q} Z^0 X$ | $3139 \pm 49$ |
| $ep \to W^+ W^- X$ | $1805 \pm 55$ |
| $ep \to q\bar{q}' W^\pm X$ | $17114 \pm 150$ |
| $\sqrt{s} = 1.36$ TeV | MRS (A) |

(b)

| $W^+W^-X$ ($t$-res.) | $tbW^\pm X$ | $tbX \to bbW^+W^-X$ | $t\bar{t}X \to bbW^+W^-X$ |
|---|---|---|---|
| $809 \pm 20(707 \pm 11)$ | $1590.0 \pm 6.6(1406.9 \pm 8.5)$ | $291 \pm 16(262 \pm 18)$ | $532.6 \pm 2.0(423.4 \pm 1.0)$ |
| $758 \pm 26(704 \pm 11)$ | $1586.7 \pm 7.5(1401.8 \pm 6.2)$ | $305 \pm 22(280 \pm 20)$ | $587.2 \pm 1.0(489.5 \pm 1.1)$ |
| $783 \pm 23(714 \pm 11)$ | $1593.6 \pm 6.8(1397.3 \pm 6.3)$ | $323 \pm 20(306 \pm 21)$ | $656.2 \pm 1.1(579.2 \pm 1.1)$ |
| $783 \pm 22(705 \pm 10)$ | $1576.2 \pm 7.8(1401.3 \pm 6.1)$ | $341 \pm 34(331 \pm 22)$ | $730.2 \pm 1.4(685.6 \pm 1.1)$ |
| $789 \pm 29(708 \pm 11)$ | $1569.3 \pm 7.7(1389.8 \pm 6.4)$ | $356 \pm 36(352 \pm 26)$ | $791.2 \pm 1.0(780.5 \pm 1.2)$ |
| $\sqrt{s} = 1.36$ TeV | $\tan\beta = 1.5(30)$ | | MRS (A) |

grounds, as we are using here a more recent set of structure functions (compare to Table III in Ref. [42]), and, at the same time, we give the rates also for the additional cases $ep \to qW^+W^-(q \neq b)$ and $ep \to q\bar{q}'W^\pm(q\bar{q}' \neq t\bar{b})$. In Table VIII(a), a sum over all possible combinations of flavors (not involving top resonances) is implied everywhere. In particular, we notice how in the case of the subprocesses $b\gamma \to W^-Z^0t$+c.c. and $g\gamma \to t\bar{t}Z^0$ there are top quarks involved as well: however, as they are produced on shell in our computations, they do not have any dependence on the MSSM parameters. On the contrary, in the case of the top resonant backgrounds $tbX$, $t\bar{t}X$, $W^+W^-X$ (via $b$-initiated subprocesses) and $q\bar{q}'W^\pm X$ (for $q\bar{q}' = t\bar{b}$+c.c.) there is such a dependence. Since $\Gamma_t^{\rm MSSM}$ is function of $M_{H^\pm}$ and $\tan\beta$ (at tree level), ten different cross sections appear in Table VIII(b). The total top width in the MSSM (together with the BR's of the top quark into $bW^\pm$ and $bH^\pm$), for the two values $\tan\beta = 1.5$ and 30, is given in Table IX.

Also, we would like to stress here a few details concerning the rates for top production via $g\gamma$ fusion. The case labeled $tbW^\pm X$ corresponds to top production via the two-to-three body subprocess $g\gamma \to t\bar{b}W^-$+c.c. (including all the 8 diagrams at tree level giving a gauge invariant set), whereas $tbX \to b\bar{b}W^+W^-X$ and $t\bar{t}X \to b\bar{b}W^+W^-X$ correspond to the rates obtained for the subprocesses $g\gamma \to b\bar{b}W^+W^-$ via graphs with one (12 diagrams) or two (2 diagrams) top resonances, respectively. That is, in the case of the two-to-four body process, we considered only the amplitudes squared of two subsets of the complete set of tree-level Feynman graphs, neglecting their interference. This clearly turns out to be an approximation (and not gauge invariant). However, as single and double top production in $g\gamma \to b\bar{b}W^+W^-$ events are by far the dominant contributions we expect to reproduce quite accurately the complete calculation. In order to check the self-consistency of our results, e.g., one can take, on the one hand, the cross section for $t\bar{b}W^-X$+c.c. in case of $t\bar{t}$ [2 diagrams, yielding, e.g., at $\tan\beta = 1.5$ and $M_{A^0} = 60$ GeV, $\approx 1195$ fb] plus the one for single $t$ production [6 diagrams, with $\sigma \approx 406$ fb, for the same choice of parameters ($M_{A^0}$, $\tan\beta$) as above] and multiply these by the corresponding $B(t \to bW^\pm)$ within the MSSM (see Table IX), after dividing by two the contribution of the $t\bar{t}$-resonant part (thus avoiding problems of double counting), and, on the other hand, the sum of the rates in third and fourth column of Table VIII(b),

TABLE IX. Total top width and BR's of the decay channels $t \to bW^\pm$ and $t \to bH^\pm$ within the MSSM, for $\tan\beta = 1.5$ and 30, for the different values of $M_{H^\pm}$ corresponding to $M_{A^0} = 60$, 80, 100, 120, and 140 GeV. The total top width in the SM is $\Gamma_t^{\rm SM} \approx 1.57$ GeV. Entries are in GeV both for masses and widths.

| $M_{H^\pm}$ | $B(t \to bW^\pm)$ | $B(t \to bH^\pm)$ | $\Gamma_t^{\rm MSSM}$ |
|---|---|---|---|
| 100.0 | 0.81(0.73) | 0.19(0.27) | 1.94(2.17) |
| 113.1 | 0.85(0.78) | 0.15(0.22) | 1.84(2.02) |
| 128.1 | 0.90(0.85) | 0.10(0.15) | 1.75(1.86) |
| 144.2 | 0.95(0.92) | 0.05(0.08) | 1.66(1.71) |
| 161.2 | 0.99(0.98) | 0.01(0.02) | 1.59(1.60) |
| $M_{W^\pm} \approx 80$ GeV | | $\tan\beta = 1.5(30)$ | $m_t = 175$ GeV |

then he ends up with numbers that are "roughly" the ones within the computational errors of the others. The above approximate procedure has been adopted in order to avoid prohibitive CPU time consumes in calculating the complete $g\gamma \to b\bar{b}W^+W^-$ process (52 Feynman graphs at tree level, including Higgs boson contributions and keeping the $W^\pm$'s on shell).

In case of neutral Higgs boson production, we divide the backgrounds in continuum and discrete. The first are the ones in which the $b\bar{b}$ pair does not come from a $Z^0$ resonance (i.e., $tbX$ and $t\bar{t}X$), and the second the ones in which the $b$'s are the decay products of the $Z^0$. Following the above distinction also in the case of double and single $H^\pm$ production, it turns out that $H^\pm$ signals have only discrete backgrounds, in which the $\tau\nu_\tau$ pair comes from a decaying $W^\pm$.

Although the background rates are in some instances much larger than the corresponding signals, one has to remember that the discrete backgrounds can be potentially dangerous only in the cases $M_{\Phi^0} \approx M_{Z^0}$ and $M_{H^\pm} \approx M_{W^\pm}$, while the continuum ones should have a quite flat distribution in the $M_{b\bar{b}}$ spectrum, where $M_{b\bar{b}}$ is the invariant mass of the $b\bar{b}$ pair. As the aim of a phenomenological analysis is to finally select signal candidate events in a window around the Breit-Wigner resonance of the Higgs bosons, we will ask that,[12] say, $|M_{\Phi^0(H^\pm)} - M_{b\bar{b}(\tau\nu_\tau)}| < 5$ GeV. If we naively assume that the invariant mass spectra of the discrete backgrounds are all contained in the regions $|M_{Z^0} - M_{b\bar{b}}| \leq 2\Gamma_{Z^0} = 5$ GeV and $|M_{W^\pm} - M_{\tau\nu_\tau}| \leq 2\Gamma_{W^\pm} \approx 5$ GeV, then the fraction of $Z^0/W^\pm$ resonant background events which overlap signal events is given by [56]

$$\delta\sigma(Z^0/W^\pm) = \sigma(Z^0/W^\pm)\frac{\max(0, 10\text{ GeV} - |M_{\Phi^0/H^\pm} - M_{Z^0/W^\pm}|)}{10\text{ GeV}}, \tag{35}$$

for $\Phi^0 = H^0$, $h^0$, and $A^0$. In using the above equation we tacitly assumed that also the $\Phi^0 \to b\bar{b}$ and $H^\pm \to \tau\nu_\tau$ peaks are all contained in a region of 10 GeV around the Higgs poles.[13]

In addition, in case of continuum backgrounds, as these are top-resonant processes and we are considering hadronic decays of the $W^\pm$'s, in order to further enhance the signal versus background ratio, we can impose the veto, say, $|M_{bW\to b(jj)} - m_t| > 15$ GeV. Since by the time the LEP⊗LHC collider will be operating the value of the top mass will be well determined, it is quite likely that the above constrain could reveal very efficient.

As criteria for the observability of a signal, we require a rate of $S \geq 6$ events with a significance $S/\sqrt{B} > 4$ for the detection of an isolated Higgs boson peak, while for the case of Higgs boson peaks overlapping with $Z^0$ or $W^\pm$ peaks we require $S \geq 10$ with $S/\sqrt{B} > 6$ [56].

In what follows we will concentrate only on the regions of parameter space ($M_{A^0}$, $\tan\beta$) where we have enough rates to presumably make a statistically significant analysis: say, at least $\sim 1$ fb of cross section, and we will analyze the signatures in Eqs. (28)–(34) separately.

### A. Signature $b\bar{b}b\bar{b}$

In this case we have contributions from the signals $H^0A^0X$, $h^0A^0X$, and $q\bar{q}\Phi^0$ (here $q = b, t$, with $t\bar{t}\Phi^0 \to b\bar{b}\Phi^0X$, flavors which give the whole of the cross sections in Table VII(a) and VII(b)), and from the backgrounds $Z^0Z^0X$ and $q\bar{q}Z^0X$, this latter for $q = b, t$, which yields a cross section of $\approx 110$ fb.

Here, the most interesting region in the plane ($M_{A^0}$, $\tan\beta$) is the one with $\tan\beta = 30$, value for which the combination $h^0A^0$ seems to be quite promising if $M_{A^0} \approx 60$ GeV (see Table IV(b)), whereas the rates for $q\bar{q}\Phi^0$ are very large over all the intermediate spectrum of $M_{A^0}$, if $\Phi^0 = h^0$, $A^0$. In the case $q\bar{q}H^0$ rates are small if $M_{A^0} \lesssim 100$ GeV. For $\mathcal{L} = 3$ fb$^{-1}$, after a few years of running, it should be possible to accumulate some tens of $h^0A^0X$ events, practically free from backgrounds, as both the $A^0$ and $h^0$ peaks are quite distant from the $Z^0$ one. The combination $H^0A^0$ is too small for deserving experimental attention, even if it doesn't substantially contribute in a possible $A^0X$ inclusive analysis. The cases $q\bar{q}h^0$ and $q\bar{q}A^0$ give hundreds or thousands of events per year, which should be easily recognized if $M_{h^0}, M_{A^0} \neq M_{Z^0}$. In the case of overlapping $Z^0$ and $h^0/A^0$ peaks, Higgs boson signal could be recognized in the form of an excess of $b\bar{b}$ events at the $Z^0$ peak. For $q\bar{q}H^0$, as $M_{H^0} - M_{Z^0} \gg 10$ GeV in the range where $H^0$ rates are large, there should not be any problem in selecting the signal. The case $\tan\beta = 1.5$ seems to be quite discouraging for all the above signals.

As this signature involves four $b$ quarks it is crucial that high $b$-tagging performances can be achieved.

[12] We do not repeat here the considerations which induced us to adopt a relatively high mass resolution, as they have been discussed for the case of the SM analysis. For this, we again refer the reader to Ref. [42].

[13] In fact, the largest Higgs boson width in the region of the parameter space here considered happens for the heavy scalar $H^0$, at $M_{A^0} = 140$ GeV and for $\tan\beta = 30$, giving $\Gamma_{H^0} \approx 2.9$ GeV.

### B. Signature $jjb\bar{b}$

This channel receives contributions from the signals $W^{\pm}\Phi^0X$ and $Z^0\Phi^0X$. The case $q\bar{q}\Phi^0$ for light flavors $q = u, d, s$, and $c$ practically does not give any event for all $\Phi^0$'s, as the bulk of the cross sections come from the subprocesses $q\bar{q}\Phi^0$ with $q = b, t$, which give the already considered $4b$ signature. The backgrounds are $W^{\pm}Z^0X$, $Z^0Z^0X$, and $q\bar{q}Z^0X$ for $q \neq b, t$, which yields a cross section of $\approx 3000$ fb. In addition, the continuum processes $tbX \to b\bar{b}W^{\pm}X$ and $t\bar{t}X \to b\bar{b}W^{\pm}X$ enter here as well (with[14] $W^{\pm} \to jj$).

Because of the small rates, we did not consider here $A^0$ production at $\tan\beta = 1.5$. Once one multiplies the rates of signal and backgrounds by the BR's giving the signature $jjb\bar{b}$, by the yearly luminosity $\mathcal{L} = 3$ fb$^{-1}$ and picks up events in the windows $|M_{b\bar{b}} - M_{\Phi^0}| < 5$ GeV, it comes out that the only case which can give significancies large enough to allow for possible detection is for $\Phi^0 = h^0$ at $\tan\beta = 1.5$. The value of $S/\sqrt{B}$ is approximately 4 over all the range 56 GeV$\lesssim M_{h^0} \lesssim$ 81 GeV. The case $\Phi^0 = H^0$ at $\tan\beta = 30$, which has production rates comparable to the ones of the previous case, is overwhelmed by the $tbX$ and $t\bar{t}X$ backgrounds (both productions rates and BR's into $b\bar{b}$ pairs are in fact smaller with respect to the light neutral Higgs boson). Therefore, in the channel $jjb\bar{b}$ only the $h^0$ scalar can be detected, and only for large $\tan\beta$'s.

### C. Signature $\tau\nu_\tau b\bar{b}$

In this case, we have to consider $H^{\pm}\Phi^0X$, $tbH^{\pm} \to b\bar{b}H^{\pm}X$ as signals, and $W^{\pm}Z^0X$ and $tbW^{\pm} \to b\bar{b}W^{\pm}X$ for backgrounds. Here, the distinction between signal and background is subtle, as the final state $tbH^{\pm}$ enters as signal for the decay $H^{\pm} \to \tau\nu_\tau$ but as background for $\Phi^0 \to b\bar{b}$ because of the top decay $t \to bX$. In the signal versus background analysis we treated the rates of $tbH^{\pm}$ exactly on this footing: when we compute the numbers for the signals separately, $tbH^{\pm}$ was considered background to $H^{\pm}\Phi^0X$, whereas, in the "inclusive" case $H^{\pm}X$ (i.e., when we summed up the rates of $H^{\pm}\Phi^0X$ and $tbH^{\pm} \to b\bar{b}H^{\pm}X$), they contributed to the event rates only. In computing the signal-to-noise ratios we ignored the case of the $H^0$ in $H^{\pm}\Phi^0X$ (whose rates are never greater than $\approx 0.4$ fb).

For the two values $\tan\beta = 1.5$ and 30 and in the range 60 GeV$\lesssim M_{A^0} \lesssim$ 140 GeV the mass of the charged Higgs boson is always larger than $\approx 100$ GeV. Therefore $W^{\pm}$ and $H^{\pm}$ peaks do not overlap in the spectrum of the invariant mass $M_{\tau\nu_\tau}$ and charged Higgs boson signal should be clearly recognized, whereas the case $H^{\pm}\Phi^0X$ is largely covered by the backgrounds (we found that significancies are always smaller than 1 after one year of running). So, the signature $\tau\nu_\tau b\bar{b}$ definitely gives large chances of charged Higgs boson detection (for all masses and $\tan\beta$'s), whereas this latter is hopeless in the case of neutral Higgs bosons.

### D. Signature $\tau\nu_\tau\tau\nu_\tau$

This channel has signal contributions from double charged Higgs boson production $H^+H^-X$ and backgrounds from charged vector boson production $W^+W^-X$, as well as from neutral production $Z^0Z^0X$ (with one $Z^0$ decaying to $\tau^+\tau^-$ pairs and the other to neutrinos). Both the processes with $H^{\pm}$'s and $W^{\pm}$'s benefit from a large top-resonant component [$q = b$ in Eq. (24)], but only background rates have significant contributions for $q \neq b$. The case $Z^0Z^0X$ has a much smaller cross section. A few words are needed here to discuss the strategy for detecting Higgs boson signals, as the presence of two neutrinos should prevent from reconstructing invariant mass spectra. For example, one possibility could simply be the one of looking at the total rates in $\tau\nu_\tau\tau\nu_\tau$ events. An excess of $2\tau 2\nu_\tau$ events (i.e., a breaking of the $\tau$ vs $\mu/e$ universality), with respect to the numbers expected from $W^+W^-X$ plus $Z^0Z^0X$ production, could well be the method of establishing the presence of $H^{\pm}$ signals. In that way, these latter should be clearly disentangled over all the intermediate mass range, for both values of $\tan\beta = 1.5$ and 30, presumably after just one year of running.

### E. Signature $jj\tau\nu_\tau$

To this channel there is a signal contribution coming from $q\bar{q}'H^{\pm}X$ when $q\bar{q}' \neq t\bar{b}$, whereas backgrounds come from $W^{\pm}Z^0X$ (with $Z^0 \to jj$) and $W^+W^-X$ events (with one $W^{\pm} \to jj$). As $M_{H^{\pm}} - M_{W^{\pm}} \gtrsim 20$ GeV over the $(M_{A^0}, \tan\beta)$ region here considered, the detection of $H^{\pm}$ signal should only be a matter of event rates. For $\tan\beta = 1.5$ numbers are very small, $\lesssim 10^{-1}$. In Table VI(b) the cross section of the process $ep \to q\bar{q}'H^{\pm}$ for $q\bar{q}' \neq t\bar{b}$ is $\approx 23(16)$ [9] $\{7\}\langle 4\rangle$ fb, for $M_{A^0} = 60$ (80) [100] $\{120\}\langle 140\rangle$ GeV and $\tan\beta = 30$. Therefore, we expect the signature $jj\tau\nu_\tau$ to give further changes to detect MSSM charged Higgs bosons at large $\tan\beta$, generally over all the intermediate mass range of the $A^0$.

We are aware that, in order to conclude our analysis in a realistic manner, some additional steps would be necessary now. For example, the gauge bosons $W^{\pm}$ and $Z^0$ that we have kinematically constrained so far to be on shell should be allowed to decay. The same should be done for the MSSM Higgs bosons $H^0, h^0, A^0$, and $H^{\pm}$. In addition, the final state partons should be evolved

[14] It would be worth here to consider also $tbX \to b\bar{b}H^{\pm}X$ and $t\bar{t}X \to b\bar{b}H^{\pm}X$ as background, although they contain a MSSM charged Higgs boson. In fact, $H^{\pm}$'s can decay to $jj$ pairs. However, as this channel has a small branching ratio (other than originating from already suppressed $t \to bH^{\pm}$ decays, see Table IX) and as we are tacitly assuming that the two jets in the signature $jjb\bar{b}$ reproduce the $W^{\pm}(Z^0)$ mass [note that $M_{H^{\pm}} - M_{W^{\pm}(Z^0)} \gtrsim 20(10)$ GeV], we can safely neglect the two above background contributions.

into hadrons and reconstructed from the detector acceptances. Therefore, on the one hand, a clustering scheme of the jets should be adopted while, on the other hand, information about the detector design (azimuthal coverage, cell structure, etc.) and performances (in particle identification, in microvertex efficiency, etc.) should be properly included into the phenomenological simulation.

Nevertheless, we have not done all of this. We have decided not to do that for two substantial reasons, related to the subject of the kinematical acceptances. First, doing this would have required a not negligible computing effort, because of the large numbers of different processes with different kinematics here involved (both among signals and backgrounds). Second, such effort could have risked being finalized in a wrong direction, in the sense that our choice of kinematical cuts could have well been different from the one which will be imposed by the real detectors. At present, in fact, the acceptances of the detectors of the LEP⊗LHC are difficult to predict, as the most recent and complete studies on the argument only deal with simulations done for the LHC (see the ATLAS [57] and CMS [58] Technical Proposals). That is, we wonder if the detectors designed for a $pp$ machine will be the same and/or will work in the same configuration even when they will be set up around a different kind of machine, an $ep$ collider.

However, in order not to leave this issue completely unaddressed, we borrow some numbers from Ref. [42], where a complete analysis was attempted. There, cuts on the transverse momentum $p_T^i$, of at least 20 GeV, on the pseudorapidity $|\eta_i|$, less than 4.5, and on the separation, $\Delta R_{ij} = \sqrt{\Delta\eta_{ij}^2 + \Delta\varphi_{ij}^2} > 1$, were assumed [37], for all the $i$th and $j$th $b$'s and jets in the signature $b\bar{b}jj$ of the SM, which would correspond here to the one obtained in the case of process (2) for $\Phi^0 = h^0$ and $\tan\beta = 1.5$ (i.e., with $M_{h^0}$ between $\approx 60$ and $\approx 80$ GeV). We concentrate only on this case since this is the one where the effects of the (continuum) backgrounds are effective but nevertheless still do not prevent detecting $h^0$ signals.

After applying the above kinematical requirements, reduction factors of $\approx$ 16–7 for the signal $W^{\pm}\phi$, with[15] $M_\phi$ = 60–140 GeV, and of $\approx$ 14/11 for the $tbX/t\bar{t}X$ backgrounds were found. As the only differences between the SM case of Ref. [42] and the MSSM one studied here (when $M_{h^0} = M_\phi$) consists in the presence of some angular factors in the SUSY vertices of reaction (2) (see Tables X–XII in the Appendix) and different (but small) top width effects in the backgrounds (the substitution $\Gamma_t^{\rm SM} \to \Gamma_t^{\rm MSSM}$), the numbers we obtained there can be safely used for the present case too. Therefore, even though the kinematical acceptances act in the direction of favoring the backgrounds, by reducing the signal-versus-noise ratio and largely spoiling the effectiveness of the $M_{bW\to bjj}$ cut (see Ref. [42]), in our opinion such effects should not have a decisive impact on the feasibility of the $h^0$ detection in $jjb\bar{b}$ events. We think the same holds also for the other signatures, especially because there background events have discrete spectra in the invariant masses of the Higgs boson decay products, and the requirements $M_{H^\pm} \approx M_{\tau\nu_\tau}$ and/or $M_{\Phi^0} \approx M_{b\bar{b}}$ should be generally sufficient to give large significancies, such that an eventual reduction due to kinematical cuts shouldn't modify the detection strategies we indicated.

Although our analysis remains partially incomplete, we believe that the purpose of our study has been reached. This was in fact to give some hints in the direction of analyzing the impact of using back-scattered photons in $\gamma p$-initiated collisions at the proposed CERN LEP⊗LHC collider, trying to establish whether such a machine could give additional informations in the study of the Higgs boson sector of the MSSM, once the potential of the two colliders LEP and LHC (separately operating) was already fully exploited. This is especially relevant if one considers the possibility that a long gap in time between the end of the LEP and LHC era and the beginning of the NLC one could happen in the future of particle physics.

A brief summary of what we have been doing and the answers to the above considerations are left in the next section.

## SUMMARY AND CONCLUSIONS

We have studied in this paper some production mechanisms of the Higgs bosons of the MSSM (i.e., $H^0$, $h^0$, $A^0$, and $H^\pm$) and of the possible backgrounds to their signatures at the proposed LEP⊗LHC $ep$ collider at CERN.

Such a machine can be obtained by crossing an electron/positron beam from LEP with a proton one from the LHC. It should presumably run with a c.m. energy at the TeV scale and with a luminosity between one and ten inverse picobarns per year. Its discovery or detection potential in the Higgs boson sector was already analyzed for the case where the collider is assumed to operate in the $ep$ mode (i.e., via electron-quark and electron-gluon scatterings). Promising results were found for the case of Higgs bosons with intermediate mass, especially if high $b$-tagging performances can be achieved in detecting neutral Higgs bosons decaying to $b\bar{b}$ pairs. We addressed here the same matter, but assuming the accelerator working in a possible $\gamma p$ mode, with the incoming photons produced through Compton backscattering of laser light against the electron or positron beam. This technique has received a lot of attention in the past few years as a concrete possibility of setting up real $e\gamma$ and $\gamma\gamma$ interactions at $e^+e^-$ linear colliders of the next generation. Such photonic interactions are expected to take place with almost the same characteristics (in energy of the beams and in integrated luminosity) as the $e^+e^-$ ones. We studied the possibility of producing $\gamma p$ interactions at CERN as we expect the design of the LEP⊗LHC machine not to prevent the application of the laser backscattering method.

Independently of the fact that SUSY Higgs bosons could have already been found either at LEP or LHC, the CERN "$\gamma p$ machine" would have a clear importance on its own, since the fundamental interactions would take place here via $\gamma$-quark and $\gamma$-gluon scatterings, these pro-

[15]Here $\phi$ represents the SM Higgs boson and $M_\phi$ its mass.

ceeding via a large number of MSSM vertices, which can then be tested. Photons, in fact, directly couple at leading order to the MSSM (charged) Higgs boson scalars, whereas electrons or positrons do not (because of the negligible mass of the electron in the Yukawa couplings). Therefore, at the NLC, very few Higgs boson production mechanisms and a reduced number of fundamental vertices are involved.

Both the high $ep$ energy available at the LEP⊗LHC and the properties of the back-scattered photons would make the production of Higgs boson events with high rates possible. Moreover, the absence of strong interactions from the initial state, which take place at hadron colliders (via $q\bar{q}$, $gg$, and $qg$ scatterings), would make the CERN machine the first TeV environment partially free from the huge QCD noise typical of the LHC (and of the Tevatron as well). Finally, both the technology and the expenses needed in converting two machines already existing (such as LEP and LHC) and physically located in the same place (even though maybe not at the same time) has to be considered, compared to building a new one (the NLC): this could make conceivable to expect the CERN $ep$ accelerator to be operating well in advance of any future linear collider.

For obvious reasons of space (in reducing the huge amount of material to a size compatible with a journal publication) and time (in numerically computing cross sections and distributions of both signals and backgrounds), we concentrated only on a limited region of the MSSM parameter space ($M_{A^0}$, $\tan\beta$). Because of kinematical constrains imposed by the collider energy and luminosity, we studied Higgs boson scalars in the intermediate mass interval whereas, as example of two opposite situations, we chose two values at the extremes of the available range of $\tan\beta$ (that is, 1.5 and 30). Our work turns out to be incomplete then. However, as the discussion of the results has been carried on by stressing their dependence on the masses and on the couplings of the MSSM Higgs boson scalars, we expect our analysis to be easily translatable to the case in which different values of $M_{A^0}$ and/or $\tan\beta$ are adopted. Some remarks are also in order concerning the treatment of the signals, of the backgrounds and the approach to the kinematical cuts.

On the one hand, we assumed a 100% $b$-tagging efficiency, thus neglecting considering light quark and gluon jets faking $b$'s in the Higgs boson decays $\Phi^0 \to b\bar{b}$. This is obviously unrealistic but, by the time of the advent of the LEP⊗LHC, $b$-tagging performances should be very high, and not too far from the above ideal case. In addition, signals and discrete backgrounds involving Higgs bosons, $Z^0$ and $W^\pm$ decaying into $b\bar{b}$ and $\tau\nu_\tau$ (the signatures of neutral and charged Higgs boson scalars we have studied here, respectively) have been computed keeping the bosons on shell, and considering the invariant mass of their decay products to fill a region of only 10 GeV around the corresponding peak. Such an approximation should be clearly dropped in the end, in order to predict reliable numbers. However, as we clearly identified as regions of feasible detection of the MSSM Higgs boson particles especially the ones well far from the $Z^0$ and $W^\pm$ resonances, we expect the inclusion of the tails of the Breit-Wigner distributions not to substantially modify our conclusions. In fact, most of the cases in which Higgs and gauge boson peaks overlap seem to be already out of the experimental possibilities in the on-shell approximation.

On the other hand, a full analysis (including kinematical cuts, detector efficiencies, hadronization effects, etc.) was far beyond our intentions, mainly because a detailed simulation should necessarily rely on the precise knowledge of the characteristics of the LEP⊗LHC detectors, which we cannot have at the moment. In this respect, a possible way to proceed could well have been, for example, the one of taking the details needed for this study from the recent ATLAS [57] and CMS [58] Technical Proposals for the LHC, which are probably the most complete and up to date source of useful information. Nevertheless, we expect that by the time the CERN $ep$ collider will be operating, both the improvement in the techniques and the necessity to adjust the detectors in view of their best performances at a different kind of machine ($ep$ instead of $pp$), could end up indicating event selection criteria different from the ones we could suppose now. What we instead preferred to do here was to take, as example, a similar study we performed in the case of the SM in a previous paper, in order to show how in general kinematical cuts should have a decisive impact on the signal significancies only where these are very small, thus affecting only restricted regions of the MSSM parameter space here considered. Leaving practically intact in the rest of the cases the chances of Higgs boson detections and studies.

Under such premises, we demonstrated the high potential of the LEP⊗LHC. What we obtained is that in some parts of the parameter region we studied all the MSSM Higgs bosons could be contemporaneously detected (especially if a high luminosity can be achieved). However, where this does not happen, at least two of them are accessible to the experiment and it is never the case that none of the Higgs boson scalars can be recognized. For all the neutral bosons ($H^0$, $h^0$, and $A^0$) we considered the $b\bar{b}$ decay channel, whereas for the charged Higgs bosons ($H^\pm$'s) we studied the decay mode $\tau\nu_\tau$. The signatures we assumed are in $b\bar{b}b\bar{b}$, $jjb\bar{b}$, $\tau\nu_\tau b\bar{b}$, $\tau\nu_\tau\tau\nu_\tau$, and $jj\tau\nu_\tau$ events. In detail, the most favorable cases are the following.

For the heavy scalar $H^0$ good chances of detection happen when $\tan\beta = 30$ in the case of the $4b$ signature, via the production subprocess $g\gamma \to b\bar{b}H^0$, if $M_{A^0} \gtrsim 120$ GeV ($M_{H^0} \gtrsim 130$ GeV). The remaining mass range $M_{A^0} \lesssim 120$ GeV ($M_{H^0} \lesssim 130$ GeV) is quite difficult to cover, as the only possible way would be via the signature $jjb\bar{b}$, through the production processes $q\gamma \to q'W^\pm H^0$ and $q\gamma \to qZ^0H^0$ (the first one mostly), which have large production rates but small significancies (large continuum backgrounds). A high luminosity option would be needed in this case (say, tens of inverse femtobarns per year) to clearly extract $H^0$ signals. If $\tan\beta = 1.5$ the situation is even less optimistic. Only after a few years of running at the standard luminosity $\mathcal{L} = 3$ fb$^{-1}$ it should be possible to recognize a few $W^\pm H^0$ events, and these

would not be probably enough for attempting a statistically significant study. Therefore, we would conclude that for the MSSM neutral heavy scalar the parameter region at small $\tan\beta$ would remain practically uncovered, whereas the one at large $\tan\beta$'s should be accessible by the experiment if $M_{H^0} \gtrsim 130$ GeV (for a standard $\mathcal{L}$).

The light neutral Higgs boson $h^0$, even with its reduced mass if compared to $M_{H^0}$, has definitely much more chances to be detected. The production in events $W^\pm h^0 X$ (giving the signature $jjb\bar{b}$) is quite large if $\tan\beta = 1.5$. As $M_{Z^0} - M_{h^0} \gtrsim 10$ GeV over all the interval 60 GeV $\lesssim M_{A^0} \lesssim 140$ GeV and the cut in $M_{bW\to bjj}$ can be successfully exploited in rejecting $tbX$ and $t\bar{t}X$ events, $h^0$ signals should be disentangled from the backgrounds up to the maximum value of $M_{h^0} \approx 81$ GeV. A few units of events per year in the above signature would come from $Z^0 h^0 X$ production too. The cases of $H^\pm h^0 X$, $h^0 A^0 X$, and $q\bar{q}h^0 X$ production do not deserve much attention (very small cross sections). If $\tan\beta = 30$, good candidates are $W^\pm h^0 X$ events, provided that $M_{h^0} \gtrsim 120$ GeV ($M_{A^0} \gtrsim 120$ GeV). The most probable signature would be again $jjb\bar{b}$. The case $Z^0 h^0 X$ at $\tan\beta = 30$ is completely beyond any experimental possibility. Production events of the type $H^\pm h^0 X$ and $h^0 A^0 X$ contribute by adding some more chances of $h^0$ detection if $\tan\beta = 30$ only in the case $M_{h^0} \approx M_{A^0} \approx 60$ GeV (via the signatures $\tau\nu_\tau b\bar{b}$ and $b\bar{b}b\bar{b}$, respectively). The case where the rewards for $h^0$ detection at high $\tan\beta$'s are largest is probably via the subprocess $g\gamma \to b\bar{b}h^0$, if $M_{h^0} \approx M_{A^0} \lesssim 120$ GeV. The production rates are in fact extremely large and the $4b$ signature is clean from backgrounds, provided that high $b$-tagging performances can be achieved and $M_{h^0}$ is far enough from $M_{Z^0}$. Therefore, for the MSSM neutral light scalar, we conclude that both the regions $\tan\beta = 1.5$ and 30 are adequately covered, and $h^0$ signals are observable.

The pseudoscalar Higgs boson $A^0$ is practically uncovered if $\tan\beta = 1.5$ and $M_{A^0} \gtrsim 80$ GeV. In fact, a few chances at small $\tan\beta$'s occur only when $M_{A^0} \approx 60$ GeV, via the signature $\tau\nu_\tau b\bar{b}$ in $H^\pm A^0 X$ events and only after a few years of running. The large $\tan\beta$ region case is instead entirely covered via the $g\gamma \to b\bar{b}A^0$ production mechanism. Even in the case that the final efficiencies and purities in $b$ tagging are smaller than the ones expected now, the large production rates should guarantee the detection of the $A^0$ in the $4b$ mode. In the case of the MSSM neutral pseudoscalar Higgs boson then, only the large $\tan\beta$ region is fully covered, whereas the remaining one is really difficult, as even the most favorable case $M_{A^0} \approx 60$ GeV needs a lot of integrated luminosity.

Finally, the case of the charged Higgs bosons. Both single and double $H^\pm$ production give account of large production rates, at both $\tan\beta$'s. As $M_{H^\pm} - M_{W^\pm} \gtrsim 10$ GeV, backgrounds should be manageable. Therefore, we expect that in the intermediate mass range of the $A^0$ (which correspond to the values 100 GeV $\lesssim M_{H^\pm} \lesssim 160$ GeV) charged Higgs bosons should be recognized and detected, both at small and at large values of $\tan\beta$.

In conclusion then, although we recognize that a more complete study (especially involving a coverage of the whole MSSM parameter space) is needed, together with a more refined signal versus background analysis (once the performances expected from the detectors of the LEP⊗LHC will become clear), we stress that the possibilities of the proposed CERN $ep$ collider in testing the Higgs boson sector of the MSSM are encouraging indeed, with the machine operating in the $\gamma p$ mode. Therefore, such a project should be seriously kept into consideration, especially if LEP and LHC together will not be able to confirm or rule out with certainty the MSSM.

TABLE X. Neutral MSSM Higgs boson couplings to each other, to the gauge bosons $W^\pm$, $Z^0$, and $\gamma$, and to the MSSM $H^\pm$'s.

| | $H^0$ | $h^0$ | $A^0$ |
|---|---|---|---|
| $W^\pm W^\mp$ | $\frac{M_{W^\pm} c_{\beta\alpha}}{s_W}$ | $\frac{M_{W^\pm} s_{\beta\alpha}}{s_W}$ | 0 |
| $H^\pm H^\mp$ | $\frac{M_{W^\pm}}{s_W}\left(c_{\beta\alpha} - \frac{1}{2c_W^2} c_{2\beta} c_{\alpha\beta}\right)$ | $\frac{M_{W^\pm}}{s_W}\left(s_{\beta\alpha} + \frac{1}{2c_W^2} c_{2\beta} s_{\alpha\beta}\right)$ | 0 |
| $W^\pm H^\mp(\gamma)$ | $\frac{s_{\beta\alpha}}{2s_W}$ | $-\frac{c_{\beta\alpha}}{2s_W}$ | $-\frac{i}{2s_W}$ |
| $Z^0 Z^0$ | $\frac{M_{W^\pm}}{s_W c_W^2} c_{\beta\alpha}$ | $\frac{M_{W^\pm}}{s_W c_W^2} s_{\beta\alpha}$ | 0 |
| $Z^0 A^0$ | $\frac{i}{2s_W c_W} s_{\beta\alpha}$ | $-\frac{i}{2s_W c_W} c_{\beta\alpha}$ | 0 |
| $H^0 H^0$ | $\frac{3M_{W^\pm}}{2s_W c_W^2} c_{2\alpha} c_{\alpha\beta}$ | $-\frac{M_{W^\pm}}{2s_W c_W^2}(2s_{2\alpha} c_{\alpha\beta} + c_{2\alpha} s_{\alpha\beta})$ | 0 |
| $H^0 h^0$ | $-\frac{M_{W^\pm}}{2s_W c_W^2}(2s_{2\alpha} c_{\alpha\beta} + c_{2\alpha} s_{\alpha\beta})$ | $\frac{M_{W^\pm}}{2s_W c_W^2}(2s_{2\alpha} s_{\alpha\beta} - c_{2\alpha} c_{\alpha\beta})$ | 0 |
| $H^0 A^0$ | 0 | 0 | $-\frac{M_{W^\pm}}{2s_W c_W^2} c_{2\beta} c_{\alpha\beta}$ |
| $h^0 h^0$ | $\frac{M_{W^\pm}}{2s_W c_W^2}(2s_{2\alpha} s_{\alpha\beta} - c_{2\alpha} c_{\alpha\beta})$ | $\frac{2M_{W^\pm}}{2s_W c_W^2} c_{2\alpha} s_{\alpha\beta}$ | 0 |
| $h^0 A^0$ | 0 | 0 | $\frac{M_{W^\pm}}{2s_W c_W^2} c_{2\beta} s_{\alpha\beta}$ |
| $A^0 A^0$ | $-\frac{M_{W^\pm}}{2s_W c_W^2} c_{2\beta} c_{\alpha\beta}$ | $\frac{M_{W^\pm}}{2s_W c_W^2} c_{2\beta} s_{\alpha\beta}$ | 0 |

TABLE XI. Charged MSSM Higgs boson couplings to the gauge bosons $Z^0$ and $\gamma$ (here $c_{2W} \equiv \cos 2\theta_W$).

| | $H^{\pm}H^{\mp}$ |
|---|---|
| $\gamma$ | 1 |
| $Z^0$ | $\frac{1}{2s_W c_W} c_{2W}$ |
| $\gamma\gamma$ | $-2$ |
| $\gamma Z^0$ | $-\frac{c_{2W}}{s_W c_W}$ |


## ACKNOWLEDGMENTS

We are grateful to J. B. Tausk for interesting discussions and useful suggestions during the early stages of this work, to T. Stelzer for his helpful advice in using MADGRAPH and, finally, to W. J. Stirling for reading the manuscript. This work was supported in part by Ministero dell' Università e della Ricerca Scientifica (S.M.), by the University of Durham and the World Laboratory (G.A.L.).


## APPENDIX

In this section we give the explicit formulas for the helicity amplitudes of the signal processes we have studied. Definitions of $S$, $Y$, and $Z$ functions and of other quantities $(p, \lambda, \mu, \eta)$ which enter in the following, can be found in Ref. [28], with identical notations, whereas definitions of the coefficients $b_i, i = 1, \ldots, 7$, of the incoming/outgoing four-momenta, of the propagators $D_V(p) = 1/(p^2 - M_V^2)$ and $D_q(p) = 1/(p^2 - m_q^2)$, $V = W^{\pm}, H^{\pm}, Z^0$, or $\gamma$ and $q = u$ or $d$, of the gluon ($i = 1$) and the photon ($i = 2$) normalization factors $N_i$, of the four-momenta $r_1, r_2, p_6$, and $p_7$ can be found in the Appendix of Ref. [42].

We introduce here the mass relation

$$\Delta^V_{\Phi,\Phi'} = \frac{M_\Phi^2 - M_{\Phi'}^2}{M_V^2} \text{ if } \Phi \neq \Phi'(M_V \neq 0),$$
$$= 0 \text{ if } \Phi = \Phi', \tag{A1}$$

and the additional coefficients

$$c^V_{\Phi,\Phi';i} = (1 - \Delta^V_{\Phi,\Phi'}) b_i, \text{ for } i = 4 \text{ and } 6,$$
$$c^V_{\Phi,\Phi';i} = -(1 + \Delta^V_{\Phi,\Phi'}) b_i, \text{ for } i = 5 \text{ and } 7, \tag{A2}$$

where $V$ and $\Phi, \Phi'$ represent vector and Higgs bosons, respectively. Definitions of the spinor functions $\mathcal{X}, \mathcal{Y}, \mathcal{Z}, \mathcal{F}$ and of their properties are the same ones of Ref. [42].[16] The MSSM couplings $c_R$, $c_L$, and $\mathcal{H}$ can be easily deduced from Tables X–XII, whereas for the SM ones we refer to [42].

### 1. Process $d\gamma \to uW^-\Phi^0$

In order to obtain from Fig. 1 the Feynman graphs of the process

$$d(p_1, \lambda_1) + \gamma(p_2, \lambda_2) \to u(p_3, \lambda_3) + W^-(p_4) + \Phi^0(p_5), \tag{A3}$$

where $\Phi^0 = H^0, h^0$ or $A^0$, one has to make the following assignments:

$$q = d, \; q' = u, \; V^{(*)} = W^{\pm(*)}, \; S^* = H^{\pm *}. \tag{A4}$$

The corresponding matrix element, summed over final spins and averaged over initial ones, is given by

$$|\bar{M}| = \frac{e^6}{4} N_2^2 \frac{3}{8\pi M_{W^\pm}^2} \sum_{\{\lambda\}} \int d\Omega_{r_2(r_2)} \sum_{l,m=1}^{17} T_l^{\{\lambda\}} T_m^{\{\lambda\}*}, \tag{A5}$$

where

$$iT_1^{\{\lambda\}} = D_u(p_3 + p_5) D_d(p_1 + p_2) M_1^{\{\lambda\}} \mathcal{H}_1, \; iT_2^{\{\lambda\}} = D_d(p_3 + p_4) D_d(p_1 + p_2) M_2^{\{\lambda\}} \mathcal{H}_2,$$
$$iT_3^{\{\lambda\}} = D_d(p_3 + p_4) D_d(p_1 - p_5) M_3^{\{\lambda\}} \mathcal{H}_3, \; iT_4^{\{\lambda\}} = D_u(p_3 + p_5) D_u(p_1 - p_4) M_4^{\{\lambda\}} \mathcal{H}_4,$$
$$iT_5^{\{\lambda\}} = D_u(p_3 - p_2) D_u(p_1 - p_4) M_5^{\{\lambda\}} \mathcal{H}_5, \; iT_6^{\{\lambda\}} = D_u(p_3 - p_2) D_d(p_1 - p_5) M_6^{\{\lambda\}} \mathcal{H}_6,$$
$$iT_7^{\{\lambda\}} = D_{W^\pm}(p_4 + p_5) D_d(p_1 + p_2) M_7^{\{\lambda\}} \mathcal{H}_7, \; iT_8^{\{\lambda\}} = D_{W^\pm}(p_4 + p_5) D_u(p_3 - p_2) M_8^{\{\lambda\}} \mathcal{H}_8,$$
$$iT_9^{\{\lambda\}} = D_{H^\pm}(p_4 + p_5) D_d(p_1 + p_2) M_9^{\{\lambda\}} \mathcal{H}_9, \; iT_{10}^{\{\lambda\}} = D_{H^\pm}(p_4 + p_5) D_u(p_3 - p_2) M_{10}^{\{\lambda\}} \mathcal{H}_{10},$$
$$iT_{11}^{\{\lambda\}} = D_{W^\pm}(p_2 - p_4) D_u(p_3 + p_5) M_{11}^{\{\lambda\}} \mathcal{H}_{11}, \; iT_{12}^{\{\lambda\}} = D_{W^\pm}(p_2 - p_4) D_d(p_1 - p_5) M_{12}^{\{\lambda\}} \mathcal{H}_{12},$$
$$iT_{13}^{\{\lambda\}} = D_{W^\pm}(p_1 - p_3) D_{W^\pm}(p_4 + p_5) M_{13}^{\{\lambda\}} \mathcal{H}_{13}, \; iT_{14}^{\{\lambda\}} = D_{W^\pm}(p_1 - p_3) D_{W^\pm}(p_2 - p_4) M_{14}^{\{\lambda\}} \mathcal{H}_{14},$$
$$iT_{15}^{\{\lambda\}} = D_{H^\pm}(p_1 - p_3) D_{H^\pm}(p_4 + p_5) M_{15}^{\{\lambda\}} \mathcal{H}_{15}, \; iT_{16}^{\{\lambda\}} = D_{H^\pm}(p_1 - p_3) D_{W^\pm}(p_2 - p_4) M_{16}^{\{\lambda\}} \mathcal{H}_{16},$$
$$iT_{17}^{\{\lambda\}} = D_{H^\pm}(p_1 - p_3) M_{17}^{\{\lambda\}} \mathcal{H}_{17}. \tag{A6}$$

[16] We again adopt in what follows the symbol $\{\lambda\}$ to denote a set of helicities of all external particles in a given reaction, $\sum_{\{\lambda\}}$ to indicate the usual sum over all their possible combinations, and the symbol $\sum_{i=j,k,l,\ldots}$ to indicate a sum over $j, k, l, \ldots$ with index $i$.

TABLE XII. Right and left handed couplings $(c_R, c_L)$ of $u$- (upper line) and $d$-type (lower line) quarks to the MSSM neutral Higgs bosons $H^0$, $h^0$, $A^0$, and of $ud$-quark pairs to the MSSM charged Higgs boson $H^\pm$ (both lines).

| $H^0$ | $h^0$ | $A^0$ | $H^\pm$ |
|---|---|---|---|
| $\frac{m_u}{2M_{W^\pm}s_W}\frac{s_\alpha}{s_\beta}(1,1)$ | $\frac{m_u}{2M_{W^\pm}s_W}\frac{c_\alpha}{s_\beta}(1,1)$ | $-i\frac{m_u}{2M_{W^\pm}s_W}\frac{1}{t_\beta}(1,-1)$ | $-\frac{1}{2\sqrt{2}M_{W^\pm}s_W}(m_d t_\beta, m_u/t_\beta)$ |
| $\frac{m_d}{2M_{W^\pm}s_W}\frac{c_\alpha}{c_\beta}(1,1)$ | $-\frac{m_d}{2M_{W^\pm}s_W}\frac{s_\alpha}{c_\beta}(1,1)$ | $-i\frac{m_d}{2M_{W^\pm}s_W}t_\beta(1,-1)$ | $-\frac{1}{2\sqrt{2}M_{W^\pm}s_W}(m_d t_\beta, m_u/t_\beta)$ |

We have

$$
\begin{aligned}
M_1^{\{\lambda\}} &= \sum_{\lambda=\pm}\sum_{\lambda'=\pm}\sum_{i=3,5,7}\sum_{j=1,2}(-b_i b_j)Y([3];[i];c^u_{R_{\Phi^0}},c^u_{L_{\Phi^0}})\\
&\quad\times Z([i];[j];\{1\};\{2\};c_{R_{W^\pm}},c_{L_{W^\pm}};1,1)Z([j];[1];[2];(2);c^d_{R_\gamma},c^d_{L_\gamma};1,1)\,,\\
M_2^{\{\lambda\}} &= \sum_{\lambda=\pm}\sum_{\lambda'=\pm}\sum_{i=3,4,6}\sum_{j=1,2}(-b_i b_j)Z([3];[i];\{1\};\{2\};c_{R_{W^\pm}},c_{L_{W^\pm}};1,1)\\
&\quad\times Y([i];[j];c^d_{R^{\Phi^0}},c^d_{L_{\Phi_0}})Z([j];[1];[2];(2);c^d_{R_\gamma},c^d_{L_\gamma};1,1)\,,\\
M_3^{\{\lambda\}} &= \sum_{\lambda=\pm}\sum_{\lambda'=\pm}\sum_{i=3,4,6}\sum_{j=1,5}(-b_i b_j)Z([3];[i];\{1\};\{2\};c_{R_{W^\pm}},c_{L_{W^\pm}};1,1)\\
&\quad\times Z([i];[j];[2];(2);c^d_{R_\gamma},c^d_{L_\gamma};1,1)Y([j];[1];c^d_{R_{\Phi^0}},c^d_{L_{\Phi^0}})\,,\\
M_4^{\{\lambda\}} &= \sum_{\lambda=\pm}\sum_{\lambda'=\pm}\sum_{i=3,5,7}\sum_{j=1,4,6}(-b_i b_j)Y([3];[i];c^u_{R_{\Phi^0}},c^u_{L_{\Phi^0}})\\
&\quad\times Z([i];[j];[2];(2);c^u_{R_\gamma},c^u_{L_\gamma};1,1)Z([j];[1];\{1\};\{2\};c_{R_{W^\pm}},c_{L_{W^\pm}};1,1)\,,\\
M_5^{\{\lambda\}} &= \sum_{\lambda=\pm}\sum_{\lambda'=\pm}\sum_{i=3,2}\sum_{j=1,4,6}(-b_i b_j)Z([3];[i];[2];(2);c^u_{R_\gamma},c^u_{L_\gamma};1,1)\\
&\quad\times Y([i];[j];c^u_{R_{\Phi^0}},c^u_{L_{\Phi^0}})Z([j];[1];\{1\};\{2\};c_{R_{W^\pm}},c_{L_{W^\pm}};1,1)\,,\\
M_6^{\{\lambda\}} &= \sum_{\lambda=\pm}\sum_{\lambda'=\pm}\sum_{i=3,2}\sum_{j=1,5,7}(-b_i b_j)Z([3];[i];[2];(2);c^u_{R_\gamma},c^u_{L_\gamma};1,1)\\
&\quad\times Z([i];[j];\{1\};\{2\};c_{R_{W^\pm}},c_{L_{W^\pm}};1,1)Y([j];[1];c^d_{R_{\Phi^0}},c^d_{L_{\Phi^0}})\,,\\
M_7^{\{\lambda\}} &= \sum_{\lambda=\pm}\sum_{i=1,2}(-b_i)Z([i];[1];[2];(2);c^d_{R_\gamma},c^d_{L_\gamma};1,1)\\
&\quad\times\Bigg\{Z([3];[i];\{1\};\{2\};c_{R_{W^\pm}},c_{L^\pm_W};1,1)\\
&\quad-\frac{\mathcal{X}_4}{M^2_{W^\pm}}\Bigg[\sum_{\lambda'=\pm}\sum_{j=1,2,3}(-b_j)Y([3];[j];1,1)Y([j];[i];c_{R_{W^\pm}},c_{L_{W^\pm}})\Bigg]\Bigg\}\,,\\
M_8^{\{\lambda\}} &= \sum_{\lambda=\pm}\sum_{i=2,3}(b_i)Z([3];[i];[2];(2);c^u_{R_\gamma},c^u_{L_\gamma};1,1)\\
&\quad\times\Bigg\{Z([i];[1];\{1\};\{2\};c_{R_{W^\pm}},c_{L_{W^\pm}};1,1)\\
&\quad-\frac{\mathcal{X}_4}{M^2_{W^\pm}}\Bigg[\sum_{\lambda'=\pm}\sum_{j=1,2,3}(-b_j)Y([i];[j];1,1)Y([j];[1];c_{R_{W^\pm}},c_{L_{W^\pm}})\Bigg]\Bigg\}\,,\\
M_9^{\{\lambda\}} &= \sum_{\lambda=\pm}\sum_{i=1,2}(-b_i)(-2\mathcal{X}_4)Y([3];[i];c_{R_{H^\pm}},c_{L_{H^\pm}})Z([i];[1];[2];(2);c^d_{R_\gamma},c^d_{L_\gamma};1,1)\,,\\
M_{10}^{\{\lambda\}} &= \sum_{\lambda=\pm}\sum_{i=2,3}(b_i)(-2\mathcal{X}_4)Z([3];[i];[2];(2);c^u_{R_\gamma},c^u_{L_\gamma};1,1)Y([i];[1];c_{R_{H^\pm}},c_{L_{H^\pm}})\,,
\end{aligned}
$$

$$
\begin{aligned}
M_{11}^{\{\lambda\}} &= \sum_{\lambda=\pm}\sum_{i=3,5,7}(2b_i)Y([3];[i];c^u_{R_{\Phi^0}},c^u_{L_{\Phi^0}})\\
&\times\Big[\mathcal{Z}_{24}\sum_{\lambda'=\pm}Y([i];p_2,\lambda';1,1)Y(p_2,\lambda';[1];c_{R_{W^\pm}},c_{L^\pm_W})\\
&-\mathcal{Y}_2 Z(\{1\};\{2\};[i];[1];1,1;c_{R_{W^\pm}},c_{L^\pm_W})-\mathcal{Y}_4 Z([2];(2);[i];[1];1,1;c_{R_{W^\pm}},c_{L_{W^\pm}})\Big],\\
M_{12}^{\{\lambda\}} &= \sum_{\lambda=\pm}\sum_{i=1,5,7}(-2b_i)Y([i];[1];c^d_{R_{\Phi^0}},c^d_{L_{\Phi^0}})\\
&\times\Big[\mathcal{Z}_{24}\sum_{\lambda'=\pm}Y([3];p_2,\lambda';1,1)Y(p_2,\lambda';[i];c_{R_{W^\pm}},c_{L_{W^\pm}})\\
&-\mathcal{Y}_2 Z(\{1\};\{2\};[3];[i];1,1;c_{R_{W^\pm}},c_{L_{W^\pm}})-\mathcal{Y}_4 Z([2];(2);[3];[i];1,1;c_{R_{W^\pm}},c_{L_{W^\pm}})\Big],\\
M_{13}^{\{\lambda\}} &= \mathcal{Z}_{24}(\mathcal{F}_{31}^{W^\pm}+2\mathcal{Y}_{31}^{W^\pm})-2\mathcal{X}_2\tilde{\mathcal{Z}}_{314}^{W^\pm}-(2\mathcal{Y}_4-\mathcal{X}_4)\tilde{\mathcal{Z}}_{312}^{W^\pm}\\
&-\frac{1}{M_{W^\pm}^2}[\mathcal{X}_2\mathcal{X}_4(\mathcal{Y}_{31}^{W^\pm}-\mathcal{X}_{31}^{W^\pm}-\mathcal{X}_{31}^{W^{\pm\prime}})+(p_1-p_3)^2(\mathcal{Z}_{24}\mathcal{F}_{31}^{W^\pm}+\tilde{\mathcal{Z}}_{312}^{W^\pm}\mathcal{X}_4)\\
&+2p_2\cdot(p_1-p_3)\mathcal{Z}_{24}\mathcal{F}_{31}^{W^\pm}]-\frac{1}{M_{W^\pm}^4}\{[(p_1-p_3)^2+p_2\cdot(p_1-p_3)]\mathcal{X}_4(\mathcal{Y}_2-\mathcal{Y}_2')\mathcal{F}_{31}^{W^\pm}\},\\
M_{14}^{\{\lambda\}} &= 2(\tilde{\mathcal{Y}}_{31}^{W^\pm}\mathcal{Z}_{24}-\mathcal{Y}_2\tilde{\mathcal{Z}}_{314}^{W^\pm}-\mathcal{Y}_4\tilde{\mathcal{Z}}_{312}^{W^\pm}),\\
M_{15}^{\{\lambda\}} &= 4Y([3];[1];c_{R_{H^\pm}},c_{L_{H^\pm}})\mathcal{X}_4(\mathcal{Y}_2+\mathcal{Y}_2'),\\
M_{16}^{\{\lambda\}} &= -2Y([3];[1];c_{R_{H^\pm}},c_{L_{H^\pm}})[\mathcal{Z}_{24}p_2\cdot(p_4+2p_5)-2\mathcal{Y}_2'\mathcal{Y}_4-2\mathcal{Y}_2\mathcal{X}_4],\\
M_{17}^{\{\lambda\}} &= Y([3];[1];c_{R_{H^\pm}},c_{L_{H^\pm}})\mathcal{Z}_{24}.
\end{aligned}
\tag{A7}
$$

### 2. Process $d\gamma \to dZ^0\Phi^0$

The Feynman graphs of the process

$$
d(p_1,\lambda_1)+\gamma(p_2,\lambda_2)\to d(p_3,\lambda_3)+Z^0(p_4)+\Phi^0(p_5),
\tag{A8}
$$

where $\Phi^0 = H^0, h^0$, or $A^0$, can be obtained from Fig. 1 by setting

$$
\begin{aligned}
q=q'=d,\ \ V^{(*)}&=Z^{0(*)},\\
M_i^{\{\lambda\}}&=0,\ \ i=11,\dots 17,\\
(S^*,\Phi^0)&=(A^{0*},H^0),\\
&=(A^{0*},h^0),\\
&=(H^{0*}+h^{0*},A^0).
\end{aligned}
\tag{A9}
$$

The formulas for the amplitude squared corresponding to $\Phi^0 = H^0$ and $h^0$ are practically the same as in the previous section, with the relabeling:

$$
u\to d,\ \ W^\pm\to Z^0,\ \ H^\pm\to A^0,
\tag{A10}
$$

in Eqs. (A5)–(A7). For the case $\Phi^0 = A^0$, the same relabeling still holds in Eq. (A5), whereas in Eqs. (A6)–(A7) only for $i = 1,\dots,8$. For diagrams 9 and 10, one has to introduce in Eqs. (A6)

$$
\begin{aligned}
iT_9^{\{\lambda\}} &= D_d(p_1+p_2)(D_{H^0}(p_4+p_5)M_{9,H^0}^{\{\lambda\}}\mathcal{H}_{9,H^0}\\
&\quad +D_{h^0}(p_4+p_5)M_{9,h^0}^{\{\lambda\}}\mathcal{H}_{9,H^0}),\\
iT_{10}^{\{\lambda\}} &= D_d(p_3-p_2)(D_{H^0}(p_4+p_5)M_{10,H^0}^{\{\lambda\}}\mathcal{H}_{10,H^0}\\
&\quad +D_{h^0}(p_4+p_5)M_{10,h^0}^{\{\lambda\}}\mathcal{H}_{10,h^0}),
\end{aligned}
\tag{A11}
$$

with $M_{i,S}^{\{\lambda\}}$, for $i = 9$, 10 and $S = H^0$, $h^0$, as given in Eqs. (A7) with the exchanges (A10), where $A^0 \to H^0, h^0$.

### 3. Process $d\gamma \to uH^-\Phi^0$

The Feynman diagrams of the process

$$
d(p_1,\lambda_1)+\gamma(p_2,\lambda_2)\to u(p_3,\lambda_3)+H^-(p_4)+\Phi^0(p_5),
\tag{A12}
$$

where $\Phi^0 = H^0, h^0$ or $A^0$, are depicted in Fig. 2, with the assignments:

$$q = d,\ \ q' = u,\ \ S = H^-,\ \ (\Phi, \Phi') = (H^-, \Phi^0),$$
$$V^* = W^{\pm *},\ \ S^*(S^{*'}) = H^{\pm *}(H^{\mp *}). \tag{A13}$$

The amplitude squared, summed over final spins and averaged over initial ones, is given by

$$|\bar{M}| = \frac{e^6}{4} N_2^2 \sum_{\{\lambda\}} \sum_{l,m=1}^{17} T_l^{\{\lambda\}} T_m^{\{\lambda\}*}, \tag{A14}$$

where the $T_i^{\{\lambda\}}$'s, for $i = 1, \ldots, 10$, are the same as in Eqs. (A6) except for a difference in sign, whereas

$$\begin{aligned}
-iT_{11}^{\{\lambda\}} &= D_{H^\pm}(p_2 - p_4) D_u(p_3 + p_5) M_{11}^{\{\lambda\}} \mathcal{H}_{11}, \quad -iT_{12}^{\{\lambda\}} = D_{H^\pm}(p_2 - p_4) D_d(p_1 - p_5) M_{12}^{\{\lambda\}} \mathcal{H}_{12}, \\
-iT_{13}^{\{\lambda\}} &= D_{H^\pm}(p_1 - p_3) D_{H^\pm}(p_4 + p_5) M_{13}^{\{\lambda\}} \mathcal{H}_{13}, \quad -T_{14}^{\{\lambda\}} = D_{H^\pm}(p_1 - p_3) D_{H^\pm}(p_2 - p_4) M_{14}^{\{\lambda\}} \mathcal{H}_{14}, \\
-iT_{15}^{\{\lambda\}} &= D_{W^\pm}(p_1 - p_3) D_{W^\pm}(p_4 + p_5) M_{15}^{\{\lambda\}} \mathcal{H}_{15}, \quad -iT_{16}^{\{\lambda\}} = D_{W^\pm}(p_1 - p_3) D_{H^\pm}(p_2 - p_4) M_{16}^{\{\lambda\}} \mathcal{H}_{16}, \\
&\quad -iT_{17}^{\{\lambda\}} = D_{W^\pm}(p_1 - p_3) M_{17}^{\{\lambda\}} \mathcal{H}_{17}.
\end{aligned} \tag{A15}$$

The spinor amplitudes are

$$\begin{aligned}
M_1^{\{\lambda\}} &= \sum_{\lambda=\pm} \sum_{\lambda'=\pm} \sum_{i=3,5,7} \sum_{j=1,2} (-b_i b_j) Y([3];[i];c^u_{R_{\Phi^0}}, c_{L_{\Phi^0}}) \\
&\quad \times Y([i];[j];c_{R_{H^\pm}}, c_{L_{H^\pm}}) Z([j];[1];[2];(2);c^d_{R_\gamma}, c^d_{L_\gamma};1,1), \\
M_2^{\{\lambda\}} &= \sum_{\lambda=\pm} \sum_{\lambda'=\pm} \sum_{i=3,4,6} \sum_{j=1,2} (-b_i b_j) Y([3];[i];c_{R_{H^\pm}}, c_{L_{H^\pm}}) \\
&\quad \times Y([i];[j];c^d_{R_{\Phi^0}}, c^d_{L_{\Phi^0}}) Z([j];[1];[2];(2);c^d_{R_\gamma}, c^d_{L_\gamma};1,1), \\
M_3^{\{\lambda\}} &= \sum_{\lambda=\pm} \sum_{\lambda'=\pm} \sum_{i=3,4,6} \sum_{j=1,5} (-b_i b_j) Y([3];[i];c_{R_{H^\pm}}, c_{L_{H^\pm}}) \\
&\quad \times Z([i];[j];[2];(2);c^d_{R_\gamma}, c^d_{L_\gamma};1,1) Y([j];[1];c^d_{R_{\Phi^0}}, c^d_{L_{\Phi^0}}), \\
M_4^{\{\lambda\}} &= \sum_{\lambda=\pm} \sum_{\lambda'=\pm} \sum_{i=3,5,7} \sum_{j=1,4,6} (-b_i b_j) Y([3];[i];c^u_{R_{\Phi^0}}, c^u_{L_{\Phi^0}}) \\
&\quad \times Z([i];[j];[2];(2);c^u_{R_\gamma}, c^u_{L_\gamma};1,1) Y([j];[1];c_{R_{H^\pm}}, c_{L_{H^\pm}}), \\
M_5^{\{\lambda\}} &= \sum_{\lambda=\pm} \sum_{\lambda'=\pm} \sum_{i=3,2} \sum_{j=1,4,6} (-b_i b_j) Z([3];[i];[2];(2);c^u_{R_\gamma}, c^u_{L_\gamma};1,1) \\
&\quad \times Y([i];[j];c^u_{R_{\Phi^0}}, c^u_{L_{\Phi^0}}) Y([j];[1];c_{R_{H^\pm}}, c_{L_{H^\pm}};1,1), \\
M_6^{\{\lambda\}} &= \sum_{\lambda=\pm} \sum_{\lambda'=\pm} \sum_{i=3,2} \sum_{j=1,5,7} (-b_i b_j) Z([3];[i];[2];(2);c^u_{R_\gamma}, c^u_{L_\gamma};1,1) \\
&\quad \times Y([i];[j];c_{R_{H^\pm}}, c_{L_{H^\pm}}) Y([j];[1];c^d_{R_{\Phi^0}}, c^d_{L_{\Phi^0}}), \\
M_7^{\{\lambda\}} &= \sum_{\lambda=\pm} \sum_{\lambda'=\pm} \sum_{i=4,5,6,7} \sum_{j=1,2} (-c^{W^\pm}_{H^-,\Phi^0;i} b_j) Y([3];[i];1,1) Y([i];[j];c_{R_{W^\pm}}, c_{L_{W^\pm}}) \\
&\quad \times Z([j];[1];[2];(2);c^d_{R_\gamma}, c^d_{L_\gamma};1,1), \\
M_8^{\{\lambda\}} &= \sum_{\lambda=\pm} \sum_{\lambda'=\pm} \sum_{i=2,3} \sum_{j=4,5,6,7} (b_i c^{W^\pm}_{H^-,\Phi^0;j}) Z([3];[i];[2];(2);c^u_{R_\gamma}, c^u_{L_\gamma};1,1) \\
&\quad \times Y([i];[j];1,1) Y([j];[1];c_{R_{W^\pm}}, c_{L_{W^\pm}}), \\
M_9^{\{\lambda\}} &= \sum_{\lambda=\pm} \sum_{i=1,2} (-b_i) Y([3];[i];c_{R_{H^\pm}}, c_{L_{H^\pm}}) Z([i];[1];[2];(2);c^d_{R_\gamma}, c^d_{L_\gamma};1,1), \\
M_{10}^{\{\lambda\}} &= \sum_{\lambda=\pm} \sum_{i=2,3} (b_i) Z([3];[i];[2];(2);c^u_{R_\gamma}, c^u_{L_\gamma};1,1) Y([i];[1];c_{R_{H^\pm}}, c_{L_{H^\pm}}), \\
M_{11}^{\{\lambda\}} &= \sum_{\lambda=\pm} \sum_{i=3,5,7} (b_i)(-2\mathcal{Y}_2) Y([3];[i];c^u_{R_{\Phi^0}}, c^u_{L_{\Phi^0}}) Y([i];[1];c_{R_{H^\pm}}, c_{L_{H^\pm}}), \\
M_{12}^{\{\lambda\}} &= \sum_{\lambda=\pm} \sum_{i=1,5,7} (-b_i)(-2\mathcal{Y}_2) Y([3];[i];c_{R_{H^\pm}}, c_{L_{H^\pm}}) Y[i];[1];c^d_{R_{\Phi^0}}, c^d_{L_{\Phi^0}}), \\
M_{13}^{\{\lambda\}} &= (-2\mathcal{X}_2)[2Y([3];[1];c_{R_{H^\pm}}, c_{L_{H^\pm}})],
\end{aligned}$$

$$
\begin{aligned}
M_{14}^{\{\lambda\}} &= (-2\mathcal{Y}_2)[2Y([3];[1];c_{R_{H^\pm}},c_{L_{H^\pm}})]\,,\\
M_{15}^{\{\lambda\}} &= [c^{W^\pm}_{H^-\Phi^0;4}\mathcal{Y}_2 + c^{W^\pm}_{H^-\Phi^0;5}\mathcal{Y}_2']\left[2\tilde{\mathcal{Y}}_{31}^{W^\pm} + \left(1-\frac{(p_1-p_3)^2}{M^2_{W^\pm}}\right)\mathcal{F}_{31}^{W^\pm}\right]\\
&\quad -2\mathcal{X}_2\left\{\left[\mathcal{X}_{31}^{W^\pm} - \frac{\mathcal{F}_{31}^{W^\pm}}{M^2_{W^\pm}}p_4\cdot(p_1-p_3)\right]c^{W^\pm}_{H^-\Phi^0;4} + \left[\mathcal{X}_{31}^{W^{\pm\prime}} - \frac{\mathcal{F}_{31}^{W^\pm}}{M^2_{W^\pm}}p_5\cdot(p_1-p_3)\right]c^{W^\pm}_{H^-\Phi^0;5}\right\}\\
&\quad +(p_4+p_5-2p_2)\cdot(c^{W^\pm}_{H^-\Phi^0;4}p_4 + c^{W^\pm}_{H^-\Phi^0;5}p_5)\tilde{\mathcal{Z}}_{312}^{W^\pm}\,,\\
M_{16}^{\{\lambda\}} &= (-2\mathcal{Y}_2)\left[\mathcal{F}_{31}^{W^\pm} - 2\mathcal{X}_{31}^{W^{\pm\prime}} - \frac{(p_1-p_3)\cdot(p_1-p_3-2p_5)}{M^2_{W^\pm}}\mathcal{F}_{31}^{W^\pm}\right]\,,\\
M_{17}^{\{\lambda\}} &= \tilde{\mathcal{Z}}_{312}^{W^\pm} - \frac{\mathcal{F}_{31}^{W^\pm}\mathcal{X}_2}{M^2_{W^\pm}}\,.
\end{aligned}
\tag{A16}
$$

### 4. Process $d\gamma \to d\Phi^0\Phi^{0\prime}$

The Feynman diagrams which describe the reaction

$$
d(p_1,\lambda_1)+\gamma(p_2,\lambda_2)\to d(p_3,\lambda_3)+\Phi^0(p_4)+\Phi^{0\prime}(p_5)\,,
\tag{A17}
$$

where $\Phi^0,\Phi^{0\prime} = H^0,h^0$, or $A^0$, are reported in Fig. 2, where

$$
q=q'=d,\ \ (\Phi,\Phi')=(\Phi^0,\Phi^{0\prime}),\ \ V^*=Z^{0*}\,,
$$

with

$$
M_i^{\{\lambda\}}=0,\ \ i=11,\ldots,17\,,
$$

and the combinations

$$
\begin{aligned}
(S^*,\Phi^0,\Phi^{0\prime}) &= (H^{0*}+h^{0*},H^0,H^0)\,,\\
&= (H^{0*}+h^{0*},H^0,h^0)\,,\\
&= (A^{0*},H^0,A^0)\,,\\
&= (H^{0*}+h^{0*},h^0,h^0)\,,\\
&= (A^{0*},h^0,A^0)\,,\\
&= (H^{0*}+h^{0*},A^0,A^0)\,.
\end{aligned}
\tag{A18}
$$

The amplitude squared is given by a formula identical to Eq. (A14). The expressions for the spinor functions and the propagators are the same as in Eqs. (A16) for the combinations $(A^{0*},H^0,A^0)$ and $(A^{0*},h^0,A^0)$, after the exchanges:

$$
u\to d,\ \ W^\pm\to Z^0,\ \ H^\pm\to A^0\,.
\tag{A19}
$$

For the cases in Eq. (A18) with double-flavored Higgs boson propagators, Eqs. (A15) and (A16) hold for the indices $i=1,\ldots,8$, while for diagrams 9 and 10, one has to introduce the same equations as in (A11) and the same $M_{i,S}^{\{\lambda\}}$'s, for $i=9,10$ and $S=H^0,h^0$, as given in Eqs. (A16) with the exchanges (A19), where $A^0\to H^0,h^0$.

### 5. Process $d\gamma \to dH^-H^+$

The Feynman diagrams for

$$
d(p_1,\lambda_1)+\gamma(p_2,\lambda_2)\to d(p_3,\lambda_3)+H^-(p_4)+H^+(p_5)\,,
\tag{A20}
$$

are again displayed in Fig. 2, where now

$$
\begin{aligned}
q=q'=d,\ \ (\Phi,\Phi')=(H^-,H^+),\ \ V^*&=\gamma^*+Z^{0*},\\
S^*=H^0+h^0,\ \ S^{*\prime}&=H^{\pm *}\,,\\
M_i^{\{\lambda\}}=0,\ \ \text{for } i&=2,3,6\,,
\end{aligned}
\tag{A21}
$$

and where, moreover, one has to exchange $\Phi\leftrightarrow\Phi'$ in diagram 12 and replace diagrams 13 and 15, by 14 and 16, respectively, but with $\Phi\leftrightarrow\Phi'$. The matrix element is given by the formula (A14), with propagators as those obtained for the case $(\Phi,\Phi')=(H^-,\Phi^0)$, except for

$$
iT_5^{\{\lambda\}} = D_d(p_3-p_2)D_u(p_1-p_4)M_5^{\{\lambda\}}\,,
\tag{A22}
$$

and with spinor functions as in Eqs. (A16), for $i=1,4,5$, where

$$
\begin{aligned}
&(c^q_{R_{\Phi^0}},c^q_{L_{\Phi^0}})\to(c_{L_{H^\pm}},c_{R_{H^\pm}}),\ \ q=u,d\,,\\
&(c^u_{R_\gamma},c^u_{L_\gamma})\to(c^d_{R_\gamma},c^d_{L_\gamma}),\ \ \text{in } M_5^{\{\lambda\}}\,.
\end{aligned}
\tag{A23}
$$

We give explicitly the remaining $T_i^{\{\lambda\}}$'s and $M_i^{\{\lambda\}}$'s, for $i=7,\ldots,17$. They are

$$
\begin{aligned}
iT_7^{\{\lambda\}} &= D_d(p_1+p_2)(D_\gamma(p_4+p_5)M_{7,\gamma}^{\{\lambda\}}\mathcal{H}_{7,\gamma}+D_{Z^0}(p_4+p_5)M_{7,Z^0}^{\{\lambda\}}\mathcal{H}_{7,Z^0})\,,\\
iT_8^{\{\lambda\}} &= D_d(p_3-p_2)(D_\gamma(p_4+p_5)M_{8,\gamma}^{\{\lambda\}}\mathcal{H}_{8,\gamma}+D_{Z^0}(p_4+p_5)M_{8,Z^0}^{\{\lambda\}}\mathcal{H}_{8,Z^0})\,,\\
iT_9^{\{\lambda\}} &= D_d(p_1+p_2)(D_{H^0}(p_4+p_5)M_{9,H^0}^{\{\lambda\}}\mathcal{H}_{9,H^0}+D_{h^0}(p_4+p_5)M_{9,h^0}^{\{\lambda\}}\mathcal{H}_{9,H^0})\,,\\
iT_{10}^{\{\lambda\}} &= D_d(p_3-p_2)(D_{H^0}(p_4+p_5)M_{10,H^0}^{\{\lambda\}}\mathcal{H}_{10,H^0}+D_{h^0}(p_4+p_5)M_{10,h^0}^{\{\lambda\}}\mathcal{H}_{10,h^0})\,,\\
iT_{11}^{\{\lambda\}} &= -D_{H^\pm}(p_2-p_4)D_u(p_3+p_5)M_{11}^{\{\lambda\}}\mathcal{H}_{11},\quad iT_{12}^{\{\lambda\}}=D_{H^\pm}(p_2-p_5)D_d(p_1-p_4)M_{12}^{\{\lambda\}}\mathcal{H}_{12}\,,\\
iT_{13}^{\{\lambda\}} &= -D_{H^\pm}(p_2-p_5)(D_{H^0}(p_1-p_3)M_{13,H^0}^{\{\lambda\}}\mathcal{H}_{13,H^0}+D_{h^0}(p_1-p_3)M_{13,h^0}^{\{\lambda\}}\mathcal{H}_{13,h^0})\,,\\
iT_{14}^{\{\lambda\}} &= D_{H^\pm}(p_2-p_4)(D_{H^0}(p_1-p_3)M_{14,H^0}^{\{\lambda\}}\mathcal{H}_{14,H^0}+D_{h^0}(p_1-p_3)M_{14,h^0}^{\{\lambda\}}\mathcal{H}_{14,h^0})\,,\\
iT_{15}^{\{\lambda\}} &= -D_{H^\pm}(p_2-p_5)(D_\gamma(p_1-p_3)M_{15,\gamma}^{\{\lambda\}}\mathcal{H}_{15,\gamma}+D_{Z^0}(p_1-p_3)M_{15,Z^0}^{\{\lambda\}}\mathcal{H}_{15,Z^0})\,,\\
iT_{16}^{\{\lambda\}} &= D_{H^\pm}(p_2-p_4)(D_\gamma(p_1-p_3)M_{16,\gamma}^{\{\lambda\}}\mathcal{H}_{16,\gamma}+D_{Z^0}(p_1-p_3)M_{16,Z^0}^{\{\lambda\}}\mathcal{H}_{16,Z^0})\,,\\
iT_{17}^{\{\lambda\}} &= D_\gamma(p_1-p_3)M_{17,\gamma}^{\{\lambda\}}\mathcal{H}_{17,\gamma}+D_{Z^0}(p_1-p_3)M_{17,Z^0}^{\{\lambda\}}\mathcal{H}_{17,Z^0}\,,
\end{aligned}
\tag{A24}
$$

and

$$
\begin{aligned}
M_{7,V}^{\{\lambda\}} &= \sum_{\lambda=\pm}\sum_{\lambda'=\pm}\sum_{i=4,5,6,7}\sum_{j=1,2}(-c_{H^-,H^+;i}^{V}b_j)Y([3];[i];1,1)Y([i];[j];c_{R_V}^d,c_{L_V}^d)\\
&\quad\times Z([j];[1];[2];(2);c_{R_\gamma}^d,c_{L_\gamma}^d;1,1)\,,\\
M_{8,V}^{\{\lambda\}} &= \sum_{\lambda=\pm}\sum_{\lambda'=\pm}\sum_{i=2,3}\sum_{j=4,5,6,7}(b_ic_{H^-,H^+;j}^{V})Z([3];[i];[2];(2);c_{R_\gamma}^d,c_{L_\gamma}^d;1,1)\\
&\quad\times Y([i];[j];1,1)Y([j];[1];c_{R_V}^d,c_{L_V}^d)\,,\\
M_{9,S}^{\{\lambda\}} &= \sum_{\lambda=\pm}\sum_{i=1,2}(-b_i)Y([3];[i];c_{R_S}^d,c_{L_S}^d)Z([i];[1];[2];(2);c_{R_\gamma}^d,c_{L_\gamma}^d;1,1)\,,\\
M_{10,S}^{\{\lambda\}} &= \sum_{\lambda=\pm}\sum_{i=2,3}(b_i)Z([3];[i];[2];(2);c_{R_\gamma}^u,c_{L_\gamma}^u;1,1)Y([i];[1];c_{R_S}^d,c_{L_S}^d)\,,\\
M_{11}^{\{\lambda\}} &= \sum_{\lambda=\pm}\sum_{i=3,5,7}(b_i)(-2\mathcal{Y}_2)Y([3];[i];c_{L_{H^\pm}},c_{R_{H^\pm}})Y([i];[1];c_{R_{H^\pm}},c_{L_{H^\pm}})\,,\\
M_{12}^{\{\lambda\}} &= \sum_{\lambda=\pm}\sum_{i=1,4,6}(-b_i)(-2\mathcal{Y}_2')Y([3];[i];c_{L_{H^\pm}},c_{R_{H^\pm}})Y([i];[1];c_{R_{H^\pm}},c_{L_{H^\pm}})\,,\\
M_{13}^{\{\lambda\}} &= (-2\mathcal{Y}_2')[Y([3];[1];c_{R_S}^d,c_{L_S}^d)]\,,\\
M_{14}^{\{\lambda\}} &= (-2\mathcal{Y}_2)[Y([3];[1];c_{R_S}^d,c_{L_S}^d)]\,,\\
M_{15,\gamma}^{\{\lambda\}} &= (-2\mathcal{Y}_2')[\mathcal{F}_{31}^{\gamma}-2\mathcal{X}_{31}^{\gamma}]\,,\\
M_{15,Z^0}^{\{\lambda\}} &= (-2\mathcal{Y}_2')\left[\mathcal{F}_{31}^{Z^0}-2\mathcal{X}_{31}^{Z^0}-\frac{(p_1-p_3)\cdot(p_1-p_3-2p_4)}{M_{Z^0}^2}\mathcal{F}_{31}^{Z^0}\right]\,,\\
M_{16,\gamma}^{\{\lambda\}} &= (-2\mathcal{Y}_2)[\mathcal{F}_{31}^{\gamma}-2\mathcal{X}_{31}^{\gamma'}]\,,\\
M_{16,Z^0}^{\{\lambda\}} &= (-2\mathcal{Y}_2)\left[\mathcal{F}_{31}^{Z^0}-2\mathcal{X}_{31}^{Z^{0\prime}}-\frac{(p_1-p_3)\cdot(p_1-p_3-2p_5)}{M_{Z^0}^2}\mathcal{F}_{31}^{Z^0}\right]\,,\\
M_{17,\gamma}^{\{\lambda\}} &= \tilde{\mathcal{Z}}_{312}^{d\gamma}\,,\\
M_{17,Z^0}^{\{\lambda\}} &= \tilde{\mathcal{Z}}_{312}^{dZ^0}-\frac{\mathcal{F}_{31}^{Z^0}\mathcal{X}_2}{M_{Z^0}^2}\,.
\end{aligned}
\tag{A25}
$$

### 6. Process $g\gamma \to u\bar{d}H^-$

The Feynman diagrams for

$$
g(p_1,\lambda_1)+\gamma(p_2,\lambda_2)\to u(p_3,\lambda_3)+\bar{d}(p_4,\lambda_4)+H^-(p_5)\,,
\tag{A26}
$$

are shown in Fig. 3, where

$$q = u,\ \ q' = d,\ \ \Phi = H^-,\ \ S^* = H^{\pm *}\,. \tag{A27}$$

The amplitude squared is

$$|\bar{M}| = \frac{e^4 g_s^2}{4} N_1^2 N_2^2 \sum_{\{\lambda\}} \sum_{l,m=1}^{8} T_l^{\{\lambda\}} T_l^{\{\lambda\}} T_m^{\{\lambda\}*}\,. \tag{A28}$$

The expressions for the $T_i^{\{\lambda\}}$'s are

$$\begin{aligned}
-iT_1^{\{\lambda\}} &= D_d(p_3+p_5)D_d(p_1-p_4)M_1^{\{\lambda\}}\mathcal{H}_1,\ \ -iT_2^{\{\lambda\}} = D_u(p_3-p_2)D_d(p_1-p_4)M_2^{\{\lambda\}}\mathcal{H}_2\,,\\
-iT_3^{\{\lambda\}} &= D_u(p_3-p_2)D_u(p_4+p_5)M_3^{\{\lambda\}}\mathcal{H}_3\,,\\
-iT_{i+3}^{\{\lambda\}} &= -iT_i^{\{\lambda\}}(u\leftrightarrow d; p_3\leftrightarrow p_4),\ \ i=1,\ldots,3\,,\\
-iT_7^{\{\lambda\}} &= D_{H^\pm}(p_2-p_5)D_d(p_1-p_4)M_7^{\{\lambda\}}\mathcal{H}_7,\ \ -iT_8^{\{\lambda\}} = -iT_7^{\{\lambda\}}(u\leftrightarrow d; p_3\leftrightarrow p_4)\,,
\end{aligned} \tag{A29}$$

while the spinor functions are

$$\begin{aligned}
M_1^{\{\lambda\}} &= \sum_{\lambda=\pm}\sum_{\lambda'=\pm}\sum_{i=3,5,7}\sum_{j=1,4}(-b_ib_j)Y([3];[i];c_{R_{H^\pm}},c_{L_{H^\pm}})\\
&\quad\times Z([i];[j];[2];(2);c^d_{R_\gamma},c^d_{L_\gamma};1,1)Z([j];[4];[1];(1);c^d_{R_g},c^d_{L_g};1,1)\,,\\
M_2^{\{\lambda\}} &= \sum_{\lambda=\pm}\sum_{\lambda'=\pm}\sum_{i=2,3}\sum_{j=1,4}(-b_ib_j)Z([3];[i];[2];(2);c^u_{R_\gamma},c^u_{L_\gamma};1,1)\\
&\quad\times Y([i];[j];c_{R_{H^\pm}},c_{L_{H^\pm}})Z([j];[4];[1];(1);c^d_{R_g},c^d_{L_g};1,1)\,,\\
M_3^{\{\lambda\}} &= \sum_{\lambda=\pm}\sum_{\lambda'=\pm}\sum_{i=2,3}\sum_{j=4,5,7}(-b_ib_j)Z([3];[i];[2];(2);c^u_{R_\gamma},c^u_{L_\gamma};1,1)\\
&\quad\times Z([i];[j];[1];(1);c^u_{R_g},c^u_{L_g};1,1)Y([j];[4];c_{R_{H^\pm}},c_{L_{H^\pm}})\,,\\
M_{i+3}^{\{\lambda\}} &= M_i^{\{\lambda\}}(u\leftrightarrow d; p_3\leftrightarrow p_4)\,,\ \ i=1,\ldots,3\,,\\
M_7^{\{\lambda\}} &= \sum_{\lambda=\pm}\sum_{\lambda'=\pm}\sum_{i=1,4}(-b_i)(-2\mathcal{Y}_2')Y([3];[i];c_{R_{H^\pm}},c_{L_{H^\pm}})Z([i];[4];[1];(1);c^d_{R_g},c^d_{L_g};1,1)\,,\\
M_8^{\{\lambda\}} &= -M_7^{\{\lambda\}}(u\leftrightarrow d; p_3\leftrightarrow p_4)\,.
\end{aligned} \tag{A30}$$

### 7. Process $g\gamma \to u\bar{u}\Phi^0$

The Feynman diagrams for

$$g(p_1,\lambda_1)+\gamma(p_2,\lambda_2)\to u(p_3,\lambda_3)+\bar{u}(p_4,\lambda_4)+\Phi^0(p_5)\,, \tag{A31}$$

with $\Phi^0 = H^0$, $h^0$, or $A^0$, can be obtained from Fig. 3 by

$$q = q' = u,\ \ \Phi = \Phi^0\,,$$

$$M_i^{\{\lambda\}} = 0,\ \ i = 7,8\,. \tag{A32}$$

With the exchanges

$$d\to u,\ \ H^\pm\to\Phi^0,\ \ (c_{R_{H^\pm}},c_{L_{H^\pm}})\to(c^u_{R_{\Phi^0}},c^u_{L_{\Phi^0}})\,, \tag{A33}$$

in Eqs. (A29) and (A30), the expressions for $T_i^{\{\lambda\}}$ and $M_i^{\{\lambda\}}$ $(i = 1,\ldots,6)$ can be easily obtained, while Eq. (A28) remains the same.

By trivial relabeling and sign exchanges, it is possible to obtain from the above formulas the corresponding ones of the $u$-type quark initiated processes

$$\begin{aligned}
u\gamma &\to dW^+\Phi^0\,,\\
u\gamma &\to uZ^0\Phi^0\,,\\
u\gamma &\to dH^+\Phi^0\,,\\
u\gamma &\to u\Phi^0\Phi^{0\prime}\,,\\
u\gamma &\to uH^+H^-\,,
\end{aligned} \tag{A34}$$

as for the charge conjugate reactions

$$\begin{aligned}
\bar{d}\gamma &\to \bar{u}W^+\Phi^0\,,\\
\bar{d}\gamma &\to \bar{d}Z^0\Phi^0\,,\\
\bar{d}\gamma &\to \bar{u}H^+\Phi^0\,,\\
\bar{d}\gamma &\to \bar{d}\Phi^0\Phi^{0\prime}\,,\\
\bar{d}\gamma &\to \bar{d}H^+H^-\,,
\end{aligned} \tag{A35}$$

and

$$\begin{aligned}
\bar{u}\gamma &\to \bar{d}W^-\Phi^0\,,\\
\bar{u}\gamma &\to \bar{u}Z^0\Phi^0\,,\\
\bar{u}\gamma &\to \bar{d}H^-\Phi^0\,,\\
\bar{u}\gamma &\to \bar{u}\Phi^0\Phi^{0\prime}\,,\\
\bar{u}\gamma &\to \bar{u}H^-H^+\,.
\end{aligned} \tag{A36}$$

Finally, the same can be done for obtaining the helicity amplitudes for the $g$-initiated processes

$$\begin{aligned}
g\gamma &\to d\bar{u}H^+\,,\\
g\gamma &\to d\bar{d}\Phi^0\,.
\end{aligned} \tag{A37}$$

[1] S. L. Glashow, Nucl. Phys. **22**, 579 (1961); S. Weinberg, Phys. Rev. Lett. **19**, 1264 (1967); A. Salam, *Elementary Particle Theory: Relativistic Groups and Analyticity (Nobel Symposium No. 8)*, edited by N. Svartholm (Almqvist and Wiksells, Stockholm, 1968), p. 367; P. W. Higgs, Phys. Rev. Lett. **12**, 132 (1964).

[2] For a review, see, for example, M. S. Chanowitz, Annu. Rev. Nucl. Part. Phys. **38**, 323 (1988), and references therein; M. Sher, Phys. Rep. **179**, 273 (1989), and references therein; R. N. Cahn, Proceedings of the 1990 Gif Summer School of Particle Physics, Strasbourg, France, 1990 (unpublished), and references therein; G. Altarelli, in Proceedings of XXVIth Recontre de Moriond, Electroweak Interactions and Unified Theories, Les Arcs, Savoie, France, 1991, edited by J. Trân Thanh Vân (unpublished), and references therein.

[3] For a review, see for example, H. P. Nilles, Phys. Rep. **110**, 1 (1984), and references therein; H. E. Haber and G. L. Kane, *ibid.* **117**, 75 (1985), and references therein; R. Barbieri, Riv. Nuovo Cimento **11**, 1 (1988), and references therein.

[4] G. G. Ross, in *Proceedings of Joint International Lepton-Photon Symposium and Europhysics Conference on High Energy Physics*, Geneva, Switzerland, 1992, edited by S. Hegarty *et al.* (World Scientific, Singapore, 1992), Vol. I, and references therein.

[5] ALEPH Collaboration, Searches for nonstandard neutral Higgs bosons," ALEPH Report No. 93-51, 1993 (unpublished); D. Treille, in *Proceedings of the Workshop on Physics and Experiments with Linear $e^+e^-$ Colliders*, Waikoloa, Hawaii, 1993, edited by F. Harris *et al.* (World Scientific, Singapore, 1993).

[6] J. F. Gunion, H. E. Haber, G. L. Kane, and S. Dawson, *The Higgs Hunter Guide* (Addison-Wesley, Reading, MA, 1990).

[7] P. Langacker and H. A. Weldon, Phys. Rev. Lett. **52**, 1377 (1984); H. A. Weldon, Phys. Rev. D **30**, 1547 (1984); Phys. Lett. **146B**, 59 (1984).

[8] R. Casalbuoni, D. Dominici, F. Feruglio, and R. Gatto, Nucl. Phys. **B299**, 117 (1988).

[9] *Proceedings of the ECFA Large Hadron Collider Workshop*, Aachen, Germany, edited by G. Jarlskog and D. Rein (CERN Report No. 90-10, ECFA Report No. 90-133, Geneva, Switzerland, 1990).

[10] Proceedings of the Summer Study on High Energy Physics in the 1990s, Snowmass, Colorado, 1988, edited by S. Jensen (unpublished); *Research Directions for the Decade*, Proceedings of the Summer Study, Snowmass, Colorado, 1990, edited by E. L. Berger (World Scientific, Singapore, 1991).

[11] *Proceedings of the ECFA Workshop on LEP 200*, Aachen, West Germany, 1986, edited by A. Bohm and W. Hoogland (CERN Report No. 87-08, Geneva, Switzerland, 1987).

[12] *Physics and Experiments with Linear Colliders*, Proceedings of the Workshop, Saariselkä, Finland, 1991, edited by R. Orawa, P. Eerola, and M. Nordberg (World Scientific, Singapore, 1992).

[13] *$e^+e^-$ Collisions at 500 GeV: The Physics Potential*, Proceedings of the Workshop, Munich, Annecy, Hamburg, 1991, edited by P. M. Zerwas (DESY Report No. 92-123A/B/C, Hamburg, 1992).

[14] *Proceedings of the ECFA Workshop on $e^+e^-$ Linear Colliders LC92*, Garmisch Partenkirchen, 1992, edited by R. Settles (MPI-PhE Report No. 93-14, ECFA Report No. 93-154).

[15] *Proceedings of the First Workshop on Japan Linear Collider (JLC)*, Tsukuba, Japan, 1989, edited by S. Kawabata (KEK Report No. 90-2, Tsukuba, 1990); *Proceedings of the Second Workshop on Japan Linear Collider (JLC)*, Tsukuba, Japan, 1990, edited by S. Kawabata (KEK Report No. 91-10, Tsukuba, 1991).

[16] J. Gunion, L. Roszkowski, A. Turski, H. Haber, G. Gamberini, B. Kayser, S. Novaes, F. Olness, and J. Wudka, Phys. Rev. D **38**, 3444 (1988).

[17] J. Dai, J. F. Gunion, and R. Vega, Phys. Lett. B **315**, 355 (1993).

[18] E. L. Berger *et al.*, "Solenoidal Detector Collaboration Technical Design Report," Report No. SDC-92-201, SSCL-SR-1215, 1992 (unpublished).

[19] A. Ballestrero, E. Maina, S. Moretti, and C. Pistarino, Phys. Lett. B **320**, 305 (1994).

[20] Z. Kunszt and F. Zwirner, Nucl. Phys. **B385**, 3 (1992), and references therein.

[21] A. Djouadi, J. Kalinowski, and P. M. Zerwas, in Ref. [13].

[22] S. Komamiya, Phys. Rev. D **38**, 2158 (1988).

[23] A. Djouadi, D. Haidt, and P. M. Zerwas, in Ref. [13].

[24] P. R. Burchat, D. L. Burke, and A. Petersen, Phys. Rev. D **38**, 2735 (1988); **39**, 3515(E) (1989).

[25] J. F. Gunion and H. E. Haber, *1990 DPF Summer Study on High Energy Physics*, Snowmass, Colorado, 1990 (Report No. UCD-90-25, 1990); J. F. Gunion and H. E. Haber, in Ref. [10] (1990); J. F. Gunion and H. E. Haber, Phys. Rev. D **48**, 5109 (1993).

[26] J. F. Gunion, in *The Fermilab Meeting*, Proceedings of the Meeting of the Division of Particle Fields of the APS, Batavia, Illinois, 1992, edited by C. Albright *et al.* (World Scientific, Singapore, 1993); J. F. Gunion, Report No. UCD-93-8, 1993 (unpublished).

[27] D. Bowser-Chao, K. Cheung, and S. Thomas, Phys. Lett. B **315**, 399 (1993).

[28] S. Moretti, Phys. Rev. D **50**, 2016 (1994).

[29] Proceedings of the HERA Workshop, edited by R. D. Peccei, Desy, Hamburg, 1987 (unpublished); Proceedings of the HERA Workshop, edited by W. Buchmüller and G. Ingelman, Desy, Hamburg, 1991 (unpublished).

[30] K. J. F. Gaemers, R. M. Godbole, and M. van der Horst, in Ref. [29] (1987).

[31] R. Bates and J. N. Ng, Phys. Rev. D **33**, 657 (1986).

[32] I. S. Choi, B. H. Cho, B. R. Kim, and R. Rodenberg, Phys. Lett. B **200**, 200 (1988).

[33] B. Grzadkowski and W.-S. Hou, Phys. Lett. B **210**, 233 (1988).

[34] T. Han and C. Liu, Z. Phys. C **28**, 295 (1985).

[35] B. Grzadkowski, S. Pokorski, and J. Rosiek, Phys. Lett. B **272**, 143 (1991).

[36] Particle Data Group, K. Hikasa *et al.*, Phys. Rev. D **45**, S1 (1992).

[37] G. Grindhammer, D. Haidt, J. Ohnemus, J. Vermaseren, and D. Zeppenfeld, in Ref. [9].

[38] D. A. Dicus and S. Willenbrock, Phys. Rev. D **32**, 1642 (1985).

[39] J. Blumlein, G. J. van Oldenborgh, and R. Ruckl, Nucl. Phys. **B395**, 35 (1993).

[40] J. L. Diaz-Cruz and O. A. Sampayo, Barcelona Autonoma University Report No. UAB-FT-286-92, 1992 (unpublished).

[41] K. Cheung, Phys. Lett. B **319**, 244 (1993).

[42] G. Abu Leil and S. Moretti, preceding paper, Phys. Rev. D **53**, 163 (1996).
[43] R. Kleiss and W. J. Stirling, Nucl. Phys. **B262**, 235 (1985).
[44] C. Mana and M. Martinez, Nucl. Phys. **B287**, 601 (1987).
[45] K. Hagiwara and D. Zeppenfeld, Nucl. Phys. **B274**, 1 (1986).
[46] A. D. Martin, R. G. Roberts, and W. J. Stirling, Phys. Rev. D **50**, 6734 (1994).
[47] P. N. Harriman, A. D. Martin, R. G. Roberts, and W. J. Stirling, Phys. Rev. D **42**, 798 (1990).
[48] Y. Okada, M. Yamaguchi, and T. Yanagida, Prog. Theor. Phys. Lett. **85**, 1 (1991); J. Ellis, G. Ridolfi, and F. Zwirner, Phys. Lett. B **257**, 83 (1991); **262**, 477 (1991); H. E. Haber and R. Hempfling, Phys. Rev. Lett. **66**, 1815 (1991); R. Barbieri and M. Frigeni, Phys. Lett. B **258**, 395 (1991).
[49] A. Brignole, J. Ellis, G. Ridolfi, and F. Zwirner, Phys. Lett. B **271**, 123 (1991); A. Brignole, *ibid.* **277**, 313 (1992).
[50] V. Barger, K. Cheung, R. J. Phillips, and A. L. Stange, Phys. Rev. D **46**, 4914 (1992).
[51] G. L. Kane, Proceedings of the Madison Workshop, 1979 (unpublished).
[52] J. H. Kühn, Acta. Phys. Pol. B **12**, 347 (1981); J. H. Kühn, Acta. Phys. Austr. Suppl. **XXIV**, 203 (1982).
[53] S. Moretti and W. J. Stirling, Phys. Lett. B **347**, 291 (1995); Erratum, Report No. DFTT60/94E, DTP/941104E, October 1995 (unpublished).
[54] See, for example, *Proceedings of the High Luminosities at LEP Workshop*, edited by E. Blucher *et al.* (CERN Report No. 91-02).
[55] T. Stelzer and W. F. Long, Comput. Phys. Commun. **81**, 357 (1994); E. Murayama, I. Watanabe, and K. Hagiwara, "HELAS: Helicity Amplitude Subroutines for Feynman Diagram Evaluations," KEK Report No. 91-11, 1992 (unpublished).
[56] K. Cheung, Phys. Rev. D **48**, 1035 (1993).
[57] ATLAS Technical Proposal, CERN/LHC/94-43 LHCC/P2, December 1994 (unpublished).
[58] CMS Technical Proposal, CERN/LHC/94-43 LHCC/P1, December 1994 (unpublished).